Lymph node contraction links sex-biased naive CD8 T cell decline to compromised antigen recognition

Authors: Lutz Menzel[1#], Maria Zschummel[2,3,4], Meghan J. O'Melia[1], Mårten Sandstedt[5,6,7], Hengbo Zhou[1], Pin-Ji Lei[1], Lingshan Liu[1], Hang Lee[8], Debattama R. Sen[2,3,4], Lance L. Munn[1], Lena Jonasson[5,9], Timothy P. Padera[1#]

Affiliations:

[1]Department of Radiation Oncology, Edwin L. Steele Laboratories, Massachusetts General Hospital and Harvard Medical School, Boston, USA

[2]Harvard Medical School, Boston, USA.

[3]Broad Institute of Harvard University and Massachusetts Institute of Technology, Cambridge, USA.

[4]Krantz Family Center for Cancer Research, Massachusetts General Hospital, Harvard Medical School, Charlestown, MA, USA.

[5]Department of Health, Medicine and Caring Sciences, Linköping University, Linköping, Sweden.

[6]Clinical Department of Radiology, Region Östergötland, Linköping, Sweden

[7]Center for Medical Image Science and Visualization (CMIV), Linköping University, Linköping, Sweden.

[8]Biostatistics Center, Harvard Medical School, Massachusetts General Hospital, Boston, Massachusetts

[9]Clinical Department of Cardiology, Region Östergötland, Linköping, Sweden

[#]Correspondence: tpadera@mgh.harvard.edu, lmenzel1@mgh.harvard.edu

Summary

A diverse naive CD8 T cell repertoire is essential to provide broad protection against infection and cancer. Here, we uncover a sex-biased mechanism of immune aging in which male mice exhibit early depletion of naive CD8 T cells through accelerated, antigen-agnostic differentiation into virtual memory cells. This depletion, compounded by androgen-driven thymic atrophy, leads to contraction of lymph nodes and a reduced local naive T cell repertoire, limiting antigen recognition capacity. Therapeutic thymus regeneration via androgen ablation repopulates naive CD8 T cells in lymph nodes and reinvigorates tumor recognition in middle-aged male mice. These findings reveal the crucial impact of sex and age on locoregional naive T cell repertoires in lymph nodes and suggest strategies to restore immune competence in aging males.

Introduction

Age is a dominant risk factor for cancer, with individuals over 50 accounting for 90% of cancer-related mortality. Notably, males exhibit nearly twice the incidence and mortality risk compared to females[1,2]. While recent work has begun to clarify how cancer-targeting T cell responses are shaped by biological sex[3–5] and age[6–9], the intersection of these factors remains incompletely understood. Thus, critical gaps remain in understanding the combined effect of age and sex on immune surveillance, elimination of dysplastic lesions and the efficacy of immunotherapies. Therapies that reverse the effects of biological sex and age on immune function have the possibility to improve healthy longevity.

The immune system's ability to recognize and respond to a wide array of antigens is directly linked to the number of naive T cells and their clonotypic diversity. With age, this compartment declines due to progressive thymic involution and ongoing peripheral attrition via differentiation into memory and senescent effector cells (**Figure 1A**)[10–14]**.** The decline of naive T cells has been linked to reduced vaccine responses, impaired tumor surveillance, and reduced efficacy of immunotherapies[10,15,16]. Lymph nodes (LNs) are the primary sites for initiating immune responses to locoregional antigen sources, rendering LNs essential for effective anti-cancer immunity. A decline of naive T cells causes insufficient populations in LNs, which limits encounters between locoregional antigen effectively presented by antigen-presenting cells (APCs) and cognate naive T cell clonotypes. These encounters are critical to generating adaptive immune responses and limiting them reduces antigen specific adaptive immunity[17].Thymic output peaks early in life through adolescence, serving as the principal source of naive T cells required to establish a diverse and self-tolerant peripheral T cell repertoire. While thymic involution has long been considered a feature of aging with limited impact on the adult immune system[11], recent human data suggest it has active clinical relevance leading to higher long-term risk of mortality and incidence of cancer. These data indicate that sustained thymic activity contributes to ongoing immune competence even later in life[18–20]. How the decline in naive T cells and associated thymic atrophy throughout life influence the ability of LNs to initiate adaptive anti-cancer immune responses, and whether and how this process differs by sex - particularly during middle age when cancer incidence increases - remains unclear.

In this study, we bridge this gap by analyzing naive CD8 T cell dynamics across the lifespan in females and males and measure the impact on effective antigen recognition in LNs. While thymic involution has long been considered the primary cause of T cell pool decline, we uncovered another male-biased mechanism in which LNs contract more rapidly with age. This male biased LN contraction is associated with an earlier loss of naive CD8 T cells driven by increased differentiation into antigen-agnostic virtual memory cells. Due to earlier thymic atrophy in males, this loss of naive CD8 T cells is not replenished. Ultimately this differentiation to virtual memory T cell reduces clonal diversity and impairs tumor recognition. Experimental thymus regeneration in males was able to restore naive CD8 T cell availability and improves tumor-targeted responses in middle-aged, but not aged, males. These mechanisms uncover the potential for immune regeneration strategies to mitigate age- and sex-related differential treatment responses. We believe this mechanism is pivotal for developing

novel therapeutic approaches to mitigate immune aging, particularly by addressing sex-specific vulnerabilities in naive T cell maintenance[21–25].

Results

Age and sex are critical factors for tumor draining LN-derived T cell responses to melanoma

Analysis of data from the Surveillance, Epidemiology, and End Results (SEER) program indicates that males have higher overall cancer incidence rates, including melanoma, with these differences becoming apparent in middle age **(Figure 1B,C)**. Both sexes had similar involvement of tumor-infiltrating T cells (TILs) in melanoma across age groups based on transcriptional immune scores **(Figure S1A)**. However, defining T cell differentiation states using transcriptional module scoring of canonical gene signatures **(Figure S1B-D)** in melanoma from published samples[26–29] revealed a higher relative proportion of naive-like CD8 T cells to antigen experienced (cytotoxic and exhausted) T cells within tumors from male patients compared to females. These data suggest restricted antigen specific activation in males **(Figure 1D-E)**, which could be a result of deficits in T cell priming in tumor-draining LNs (tdLNs). In addition to well-documented sex and age-related T cell impairments, such as exhaustion or the development of suppressor phenotypes[3–5,7,8], a notable proportion of TILs in older individuals also retain a naive state. Consequently, these TILs may not actively engage in, and could remain bystanders to, antitumor immune responses[28,30,31].

Studying immune mediated tumor control in mice as a function of age and sex, our data show tumor control declined dramatically from young adult to middle-aged males, whereas females have a more modest decline in CD8 T cell-dependent tumor control **(Figure 1F)**. In young adult mice, tumor growth dynamics were similar between sexes; however, middle-aged females exhibited a CD8 T cell-dependent delay in tumor growth compared to males and a stronger response to anti-PD-1 treatment, supporting a T cell-dependent sex disparity in limiting cancer progression **(Figure 1F; Figure S2A-H)**. At an early stage of tumor growth, when significant sex-related differences in tumor size were already apparent **(Figure 1G)**, we performed flow cytometric analysis of TILs in B16-OVA tumors from middle-aged mice. Consistent with patient data **(Figure 1D,E),** tumors in middle-aged females contained a higher proportion of antigen-experienced T cells ($CD44^+PD1^+$) and T cells with functional effector phenotype (Granzyme B^+), while males exhibited a predominance of naive CD8 T cells **(Figure 1H; Figure S3A,B)**. This disparity occurred despite comparable overall CD8 T cell infiltration and intratumoral proliferation of effector T cells **(Figure S3C)**. The number of exhausted T cells ($TIM3^+PD1^+$) was higher in females and regulatory T cells similar between sexes **(Figure S3D,E)**. The relative increase in naive T cells in tumors from middle-aged males suggests that they are not properly primed prior to entering the tumor.

The higher frequency of $CD44^+PD1^+$ CD8 T cells was also present in the blood of female mice, suggesting that these cells are activated outside the tumor and likely reflect more effective priming in LNs compared to males **(Figure 1I)**. We performed splenectomy (SpX) and utilized lymphotoxin alpha-deficient (*Lta*$^{-/-}$) mice, which lack functional LNs[32], and found that LNs, rather than the spleen, are critical for supporting the superior tumor recognition capacity in females **(Figure 1J)**. Consistently, tdLNs from female mice contained significantly higher numbers of antigen-

experienced (CD44⁺PD1⁺) and tumor specific (tetramer⁺) CD8 T cells, independent of the proliferation capacity of activated cells **(Figure 1K, Figure S3E,F)**, suggesting a higher probability of naive T cells to recognize tumor antigens in tdLNs of females. Together, these findings indicate that tumors in females have a higher proportion of cancer-targeting CD8 effector T cells that originate and are primed in the tdLNs and are then able to infiltrate the tumor, consistent with the human data (**Figure 1D-E**).

Of note, while sex disparities of intradermal APCs have been reported for adult mice[33], in middle-aged mice the LNs did not contain dysregulated proportions of APCs or show differences in antigen presentation between the sexes in humans or mice **(Figure S4A-E)**. This lack of sex-based differences in antigen presentation in LNs prompted us to test whether middle-aged males possess a restricted naive T cell pool and, consequently, a limited repertoire of unique TCRs capable of recognizing tumor antigens in LNs.

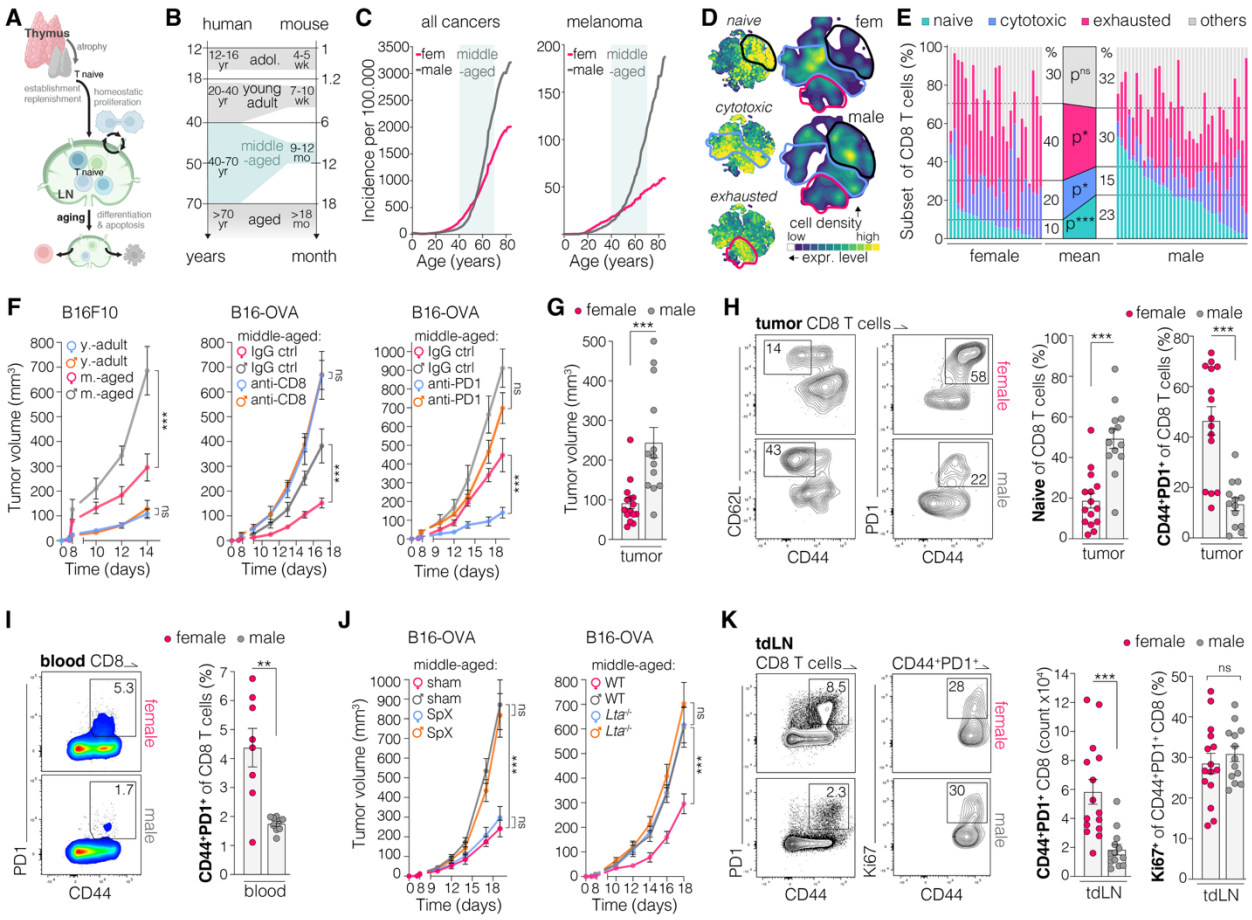

Figure 1. Age and sex are critical factors for tdLN-derived T cell responses to melanoma.
(A) Schematic illustration of naive T cell and LN homeostasis.
(B) Age categories in humans and mice.
(C) Incidence per 100,000 individuals, data from SEER (n=1.8-17.8x10^6 cases per year and sex group).
(D) Cell density projections and expression levels of module scores of CD8 T tumor infiltrating lymphocytes (TILs) isolated from melanomas from patients, integrated public data sets[1–4]. Corresponding data in **Figure S1B-E**.
(E) Frequency of CD8 T cell subsets in individual patients and in average per sex (females n=25, males n=35).

(F) B16F10 or B16-OVA tumor growth in, *left*, untreated young adult (y.-adults, n=5) or middle-aged (m.-aged, n=8) mice, *middle*, after CD8 T cell depletion (n=5/group), and *right*, with anti-PD1 checkpoint inhibition (n=5/group).
(G) B16-OVA tumor volume at the day of flow cytometry analysis, group matched 13-15 days after implantation (corresponding to **H,I**).
(H) Flow cytometry analysis of CD8 T cells isolated from B16-OVA tumors. Gating strategy in **Figure S3A**.
(I) CD8 T cells from blood of middle-aged mice with B16-OVA tumors.
(J) B16-OVA tumor growth in middle-aged mice, *left*, after sham surgery or splenectomy (SpX), n=8/group, and *right*, in wild-type (WT) or lymphotoxin alpha knock out (*Lta*$^{-/-}$) mice, n=8-10/group.
(K) Flow cytometry analysis of CD8 T cells from tumor-draining lymph nodes (tdLNs) of middle-aged mice with B16-OVA tumors 13-15 days after implantation. Gating strategy in **Figure S3A**.
Data shown as mean ± SEM with data points representing individual animals or persons. Statistics calculated with Mann-Whitney U test (MWU) test (E,G,H,I,K), 2-way ANOVA (F,J), ns=nonsignificant, *p<0.05, **p<0.01, ***p<0.005.

Age-related decline of naive CD8 T cells and contraction of LNs occur earlier in males

Volume segmentation of full-body computed tomography (CT) scans of humans from a publicly available database revealed larger spleens but significantly smaller lymph nodes (LNs) in males compared to females **(Figure 2A; Figure S5A,B)**. With age, LNs can accumulate fat due to lipomatosis, disrupting the correlation between volume and cellularity, which can potentially lead to an underestimation in the decline in cellularity[34]. In middle-aged mice, LNs did not occur with a dysregulated stromal structure **(Figure S6A)**. Consistent with human LN data, murine LN size and cellularity declined with age, occurring earlier and more markedly in males, and resulting in a significant sex disparity by middle age **(Figure 2B,C)**. The differences were more pronounced in skin-draining compared to mesenteric LNs and were independent of reproductive status and genetic background **(Figure S6B-D)**. LN weight strongly correlated with cellularity during physiological aging and under lymphopenic conditions, emphasizing the co-dependence of LN size with the number of lymphocytes **(Figure 2D; Figure S6E)**, which indicates that, despite potential confounding factors, imaging-based LN volume measurements in humans reflect underlying cellularity.

Published reports suggest that total T cell numbers, including both CD4 and CD8 T cells, remain relatively stable with age, with age-related immune remodeling largely driven by a gradual shift from naive to memory subsets[10,35]. However, our data show that CD44^{+}CD62L^{+} memory-phenotype and naive CD8 T cells begin to decline after young adulthood, with naive T cells showing an even more pronounced reduction in males compared to females (**Figure 2E**). Naive CD8 T cells also declined across other peripheral compartments, including blood, spleen, and bone marrow (BM) (**Figure 2F**). Published multimodal datasets of human T cells from blood and LNs[36–38] corroborated these findings, showing a decline of naive CD8 T cells determined by applying a gene expression "*Naive score*" on scRNA-seq and flow cytometry data **(Figure 2G,H; Figure S5C-F)**.

To examine TCR diversity in LNs, we performed TCR sequencing of CD8 T cells from LNs of middle-aged mice and found a maximally diverse TCR repertoire with over 96% of unique T cell clonotypes in non-reactive LNs independent of sex, mirroring observations in humans[38] **(Figure S7A-E)**. Thus, we hypothesized that the absolute number of naive T cells within a LN at any given time is directly correlated with the number of unique TCRs present and is therefore a rate-limiting factor for the probability of antigen recognition. To test this, we immunized middle-aged mice intradermally in the flank with either inactivated H1N1 virus particles or B16-OVA tumor cell lysates and analyzed the

draining LNs at 24- and 72-hours post-immunization to assess early T cell activation. Both sexes exhibited similar frequencies of CD8 T cells expressing the general activation marker CD69. However, a significantly greater number of CD8 T cells in females exhibited TCR-specific activation, as indicated by a higher proportion of Nur77^{+} cells[39] **(Figure 2I; Figure S7F)**. We attribute this sex imbalance to the partial depletion of naive CD8 T cells in middle-aged males and the concomitant contraction of LNs, which are central to locoregional antigen processing and recognition. These data highlight the functional impact of higher naive T cell numbers in middle-aged females on the generation of antigen specific immune responses. The greater activation of CD8 T cells in LNs of middle-aged female mice is consistent with an increase in the proportion of antigen-experienced CD8 TILs in the human data (Figure 1D-E). Even though middle-aged male mice have fewer total numbers of naïve CD8 T cells, they also have fewer antigen experienced CD8 T cells due to reduced TCR diversity in LNs. Thus, as a *proportion*, the TILs in the human data remain skewed toward a naïve phenotype.

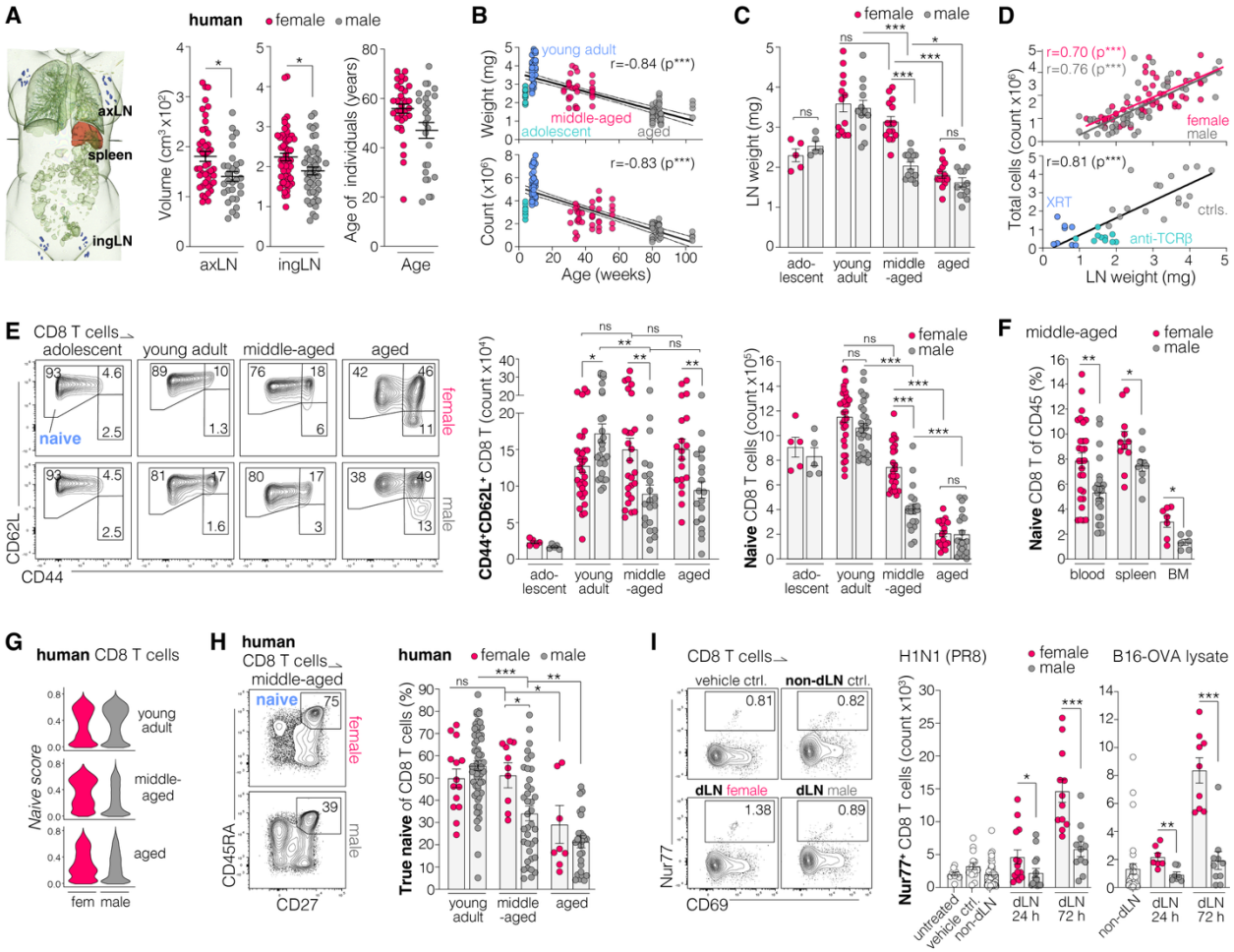

Figure 2. Age-related naive CD8 T cell decline and LN contraction occurs earlier in males.
(A) Average axillary (axLN) and inguinal (ingLN) LN volume per human individual, segmented from computer tomography (CT) scans[5,6], age of individuals (when available, for others, age is unspecified) corresponding data in **Figure S5A,B**.
(B) Correlation of LN weight or cellularity with age of mice, including female and male, adolescents excluded from correlation calculation.

(C) LN weights in age-groups of female/male mice.
(D) *Top*, correlation of LN weight to LN cellularity across all ages, *bottom*, and after irradiation (XRT, 4 Gy) or anti-T cell receptor beta chain (TCRß) antibody mediated T cell depletion.
(E) Flow cytometry analysis of naive and memory ($CD44^+CD62L^+$) CD8 T cells from ingLNs of mice. Gating strategy in **Figure S6F**.
(F) Frequency of naive CD8 T cells in the blood, spleen and bone marrow (BM).
(G) Expression levels of naive T cell genes (*Naive score*) in human CD8 T cells, ABF300 study[7]. Naive score described in **Figure S5C**.
(H) Flow cytometry quantification of true naive CD8 T cells from human PBMCs, public data set[8]. Gating Strategy in **Figure S5F**.
(I) Nur77 expression in CD8 T cells from the draining lymph node (dLN) of middle-aged mice 24 or 72 h after immunization with UV light inactivated H1N1 (PR8) influenza virus or B16F10-OVA melanoma cell lysate.
Data shown as mean ± SEM with data points representing individual animals or persons. Statistics calculated with MWU test (A,C,E,F,H,I), Pearson correlation (B,D), ns=nonsignificant, *p<0.05, **p<0.01, ***p<0.005.

Enhanced propensity for an antigen-agnostic loss of T cell naivety in males

While thymic involution is a well-known feature of aging, its functional relevance remains debated[11,20], as peripheral T cell numbers, particularly in the CD4 compartment, are thought to remain relatively stable in adulthood[40]. However, our data reveal a progressive, selective decline in naive CD8 T cells with age, suggesting that peripheral maintenance alone is insufficient. This raises the question of what drives this loss and why it occurs earlier in males.

Naive CD8 T cells are long-lived but can exit the naive pool through activation into effector and central memory (Tcm) cells upon antigen encounter, or via antigen-agnostic differentiation into virtual memory (Tvm) cells (**Figure 3A**). While the effector/Tcm route can be pathogen-driven[10,16,41], our data show that naive CD8 T cells still decline with age in mice housed in low-pathogen conditions **(Figure 2E-F)**. $CD44^+CD62L^-$ effector-like cells did not differ by sex across the lifespan (**Figure S8A**), suggesting similar antigen exposure. However, young adult males exhibit an increased frequency of $CD44^+CD62L^+$ CD8 T cells already before any sex difference in LN cellularity is apparent in middle-aged **(Figure 3B)**. Consistent with previous studies[42–44], most $CD44^+CD62L^+$ cells were not true Tcm ($CD44^+CD49d^+$), but Tvm cells ($CD44^+CD122^+CD49d^-$) **(Figure 3C,D; Figure S8B)**. The propensity of naive CD8 T cells to undergo antigen-agnostic differentiation into Tvm cells is shaped by their clone-specific sensitivity to self-peptide-MHC and is reflected by CD5 expression, which is stably imprinted during thymic selection[45–47]. $CD5^{high}$ cells are more self-reactive and more likely to undergo Tvm conversion in the periphery over time[47,48].

To test whether high self-reactivity alone is sufficient to drive this process, we used the OT-I mouse model, in which all CD8 T cells express a monoclonal TCR and have elevated affinity for endogenous self-antigens[47,48], resulting in near-uniform $CD5^{high}$ expression **(Figure 3E, Figure S8C)**. As expected, OT-I mice exhibited accelerated Tvm formation, a pronounced depletion of naive CD8 T cells in LNs, and reduced cellularity of both LNs and spleen in both sexes **(Figure 3H; Figure S8D)**. These findings confirm that high TCR self-reactivity is sufficient to drive antigen-agnostic differentiation and naive CD8 T cell pool contraction. To determine whether this mechanism operates in a physiologically diverse TCR setting, we analyzed WT mice and found that $CD5^{high}$ cells were enriched in the Tvm population relative to naive CD8 T cells **(Figure 3E,F)**, and that $CD5^{high}$ true naive CD8 T cells were

more frequent in young adult males than females, suggesting a sex-biased predisposition to early Tvm conversion.

From an evolutionary perspective, this early skewing may reflect a functional trade-off. Tvm cells offer rapid, cytokine-driven responses that prioritize short-term immune readiness over long-term repertoire maintenance. From an evolutionary perspective, such front-loaded immunity may be favored in males, while females preserve naive T cells longer to support extended immune surveillance. Consistent with the increased frequency of CD5^{high} cells in young male mice, our analysis of publicly available scRNA-seq data[36,49,50] from human single-positive (SP) CD8 thymocytes and naive CD8 T cells in PBMCs in a young adult cohort also revealed a higher frequency of CD5^{high} cells in males compared to females **(Figure 3G)**. In mice, this difference reversed with age as CD5^{high} frequencies increased in females but declined in middle-aged males, likely reflecting selective loss of self-reactive clones through prior Tvm differentiation **(Figure 3F)**.

While the difference in CD5^{high} naive CD8 T cell frequency between young adult females and males is numerically modest (approximately 0.7% vs. 1.1% of naive CD8 T cells in mice), even subtle disparities can drive a cumulative divergence in Tvm cell generation over a long period of time, like during aging. The 'skimming' of higher self-affinity clones from the naive CD8 T cell pool occurs at a higher rate early in life in males, leading to progressive depletion of this subset and a gradual enrichment of Tvm cells with age **(Figure 3I)**. LNs continue to shrink with age despite Tvm formation, as Tvm cells have a shorter lifespan due to increased rate of apoptosis[42,51], and preferential relocation to the spleen, bone marrow **(Figure S8E,F)** or liver[48]. As a result, although Tvm formation occurs in both sexes, its earlier and more rapid onset in males contributes to a sex-biased loss of naive CD8 T cells and LN contraction earlier during aging.

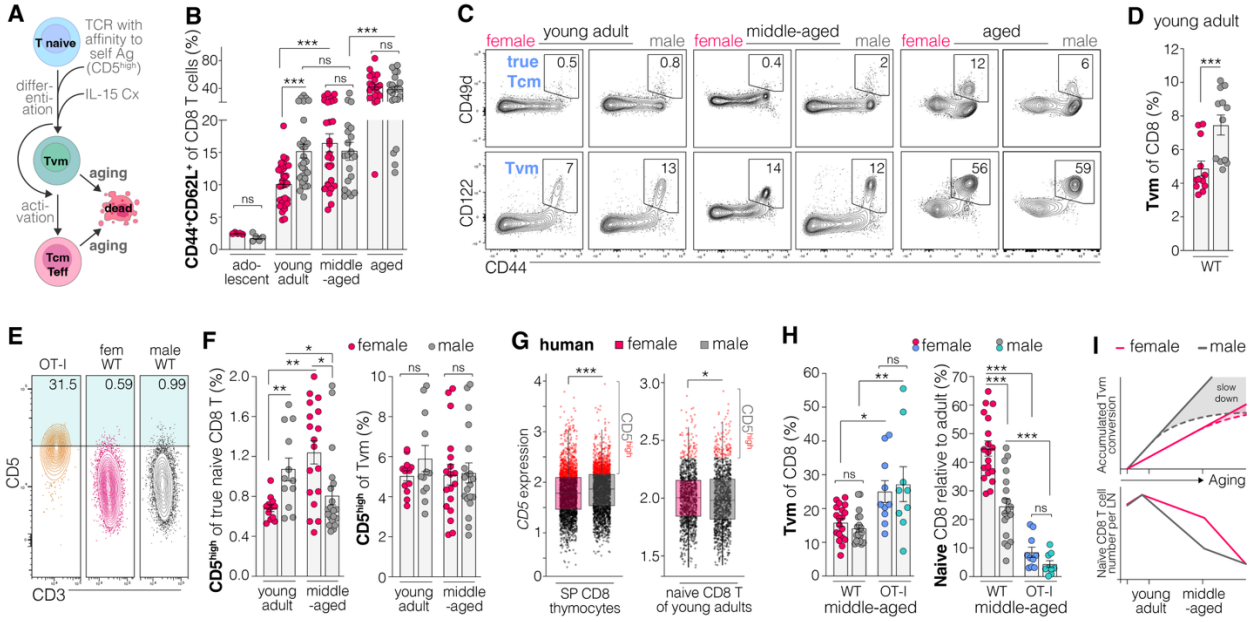

Figure 3. Enhanced propensity for antigen-inexperienced loss of T cell naivety in male mice.
(A) Schematic illustration of naive T cell differentiation into virtual memory (Tvm), effector (Teff) and central memory (Tcm) cells; T cell receptor (TCR), IL-15/IL15 receptor alpha complex (IL-15 Cx).

(B) Frequency of $CD44^+CD62L^+$ cells in ingLNs of WT mice. Example flow cytometry plots in **Figure S8D**.
(C) Flow cytometry analysis of CD8 T cells from the ingLN of adult, middle-aged and aged mice, indicated that $CD44^+CD62L^+$ contain both true Tcm and Tvm cells. Gating strategy in **Figure S6F**. Quantified in **Figure S8B**.
(D) Tvm cell percentage of CD8 T cells in young adult ingLNs.
(E) Histograms of CD5 expression in true naive CD8 T cells from ingLNs of WT or OT-I (ovalbumin-specific TCR transgenic) mice. OT-I mice were used as a known positive control that has high $CD5^{high}$ CD8 T cell population to help defining $CD5^{high}$.
(F) Quantification of $CD5^{high}$ cells from ingLNs of WT as a percent of true naive CD8 T cells or Tvms.
(G) Quantification of $CD5^{high}$ CD8 single positive or naive CD8 T cells from published datasets of human thymocytes[9,10] and PBMCs[7] shows that young adult males have more $CD5^{high}$ cells compared to females.
(H) Quantification of Tvm and naive CD8 T cells in middle-aged WT and OT-I mice show increased Tvm and reduced naive CD8 T cells in OT-I mice with no sex difference.
(I) Illustrative projection of cumulative conversion of $CD5^{high}$ naive CD8 T cells into Tvm cells during aging. *Top*, indicated are the linear accumulation of Tvm cells over time (solid line) and the assumed deceleration in accumulation due to IL-15 limitation and - and the prior conversion of naive CD8 T cells with highest CD5 levels (dashed line). *Bottom*, the Tvm formation associated attrition of naive CD8 T cells.
Data shown as mean ± SEM with data points representing individual animals. Statistics calculated with MWU test (B,D,F,H), Fisher's Exact test (G), ns=nonsignificant, *p<0.05, **p<0.01, ***p<0.005.

Transient experimental Tvm induction initiates a naive CD8 T cell decline in long-term

To further, establish that Tvm formation can lead to a depletion in naive CD8 T cell populations, we used IL-15/IL-15 receptor alpha complexes (IL-15 Cx), the biologically most active form of IL-15, to experimentally drive Tvm formation in young adult female mice. IL-15 is not a direct driver of Tvm differentiation but acts as a permissive co-stimulatory signal that in conjunction with CD5 lowers the activation threshold for naive CD8 T cells with elevated self-reactivity to convert into Tvm cells. In this way, IL-15 fine-tunes the sensitivity of the naive pool to undergo antigen-agnostic differentiation, particularly in $CD5^{high}$ clones. The frequency of $CD5^{high}$ naive CD8 T cells is lower in adult females than in males, requiring stronger IL-15 signaling to overcome the activation threshold for Tvm differentiation. Thus, using IL-15 Cx enabled us to experimentally lower the self-affinity threshold for Tvm formation in a setting with normal TCR diversity but otherwise low baseline Tvm conversion.

Recombinant IL-15 Cx was administered four times once weekly to young adult female mice (**Figure 4A**). We focused on females as a biologically informative model. Males already exhibit elevated Tvm frequencies and a reduced naive CD8 T cell pool by middle age, making it difficult to isolate cause and effect. In contrast, IL-15 Cx-treated females allowed us to ask whether transient, experimentally induced Tvm formation could mimic male-like immune aging. This approach allowed us to probe the causal link between premature Tvm skewing and later-life naive T cell loss in a setting where these features are not inherently coupled, thereby isolating the hypothesized process from confounding baseline differences. We observed a marked expansion of Tvm cells in LNs after the acute IL-15 Cx stimulation phase (4 wks.). Remarkably, this transient intervention led to a significant and lasting reduction in naive CD8 T cells seven months later (7 mo.) mimicking the profile observed in age-matched untreated male mice **(Figure 4B,C)**.

We next asked whether IL-15 Cx levels differ endogenously between sexes and might contribute to the early Tvm formation observed in males. Surprisingly, IL-15 Cx protein levels in lymph nodes were lower in young adult males than females and declined with age in both sexes **(Figure 4D)**. These differences were observed at the protein but not transcript level **(Figure S8G)**, suggesting that lower

IL-15 Cx levels in males are not the cause but a consequence of increased IL-15 consumption by a higher number of Tvm cells.

While the acute expansion of Tvm cells had no measurable effect on tumor rejection shortly after treatment (4 wks.), early-life IL-15 Cx treatment led to decreased numbers of activated CD8 T cells within tdLNs and the tumor, and reduced tumor control later in life in middle-aged mice **(Figure 4E,F)**. These findings demonstrate that transient induction of Tvm cells without disruption of anti-tumor T cell responses in the acute phase, has long-lasting consequences for immune surveillance, effectively recapitulating key features of male-biased immune aging.

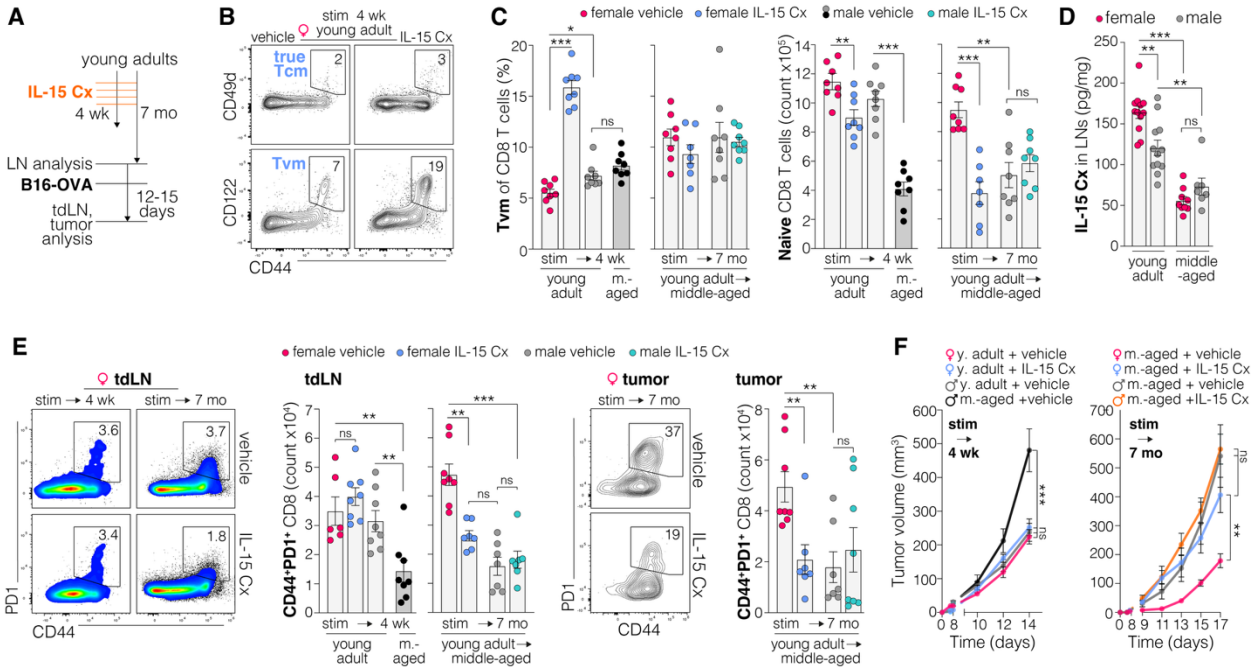

Figure 4. Experimental induction of Tvm in young females leads to restricted naive CD8 T cell pool in middle-aged.
(A) Experimental set up, young adult and middle-aged mice treated with vehicle or IL-15/IL-15 receptor alpha complex (Il-15 Cx) with LN analysis and B16-OVA tumor implantation directly after the acute stimulation phase (stim → 4 wk) or 7 months later (stim → 7 mo).
(B,C) Representative flow cytometry analysis **(B)** and quantification **(C)** of CD8 T cells in ingLNs of mice treated with vehicle or IL-15 Cx stimulation as described in **(A)**; middle-aged (m.-aged).
(D) IL-15 Cx quantification in ingLNs of adult and middle-aged mice relative to weight of the LNs.
(E) Flow cytometry analysis of CD8 T cells from the tdLNs or the primary tumor, young-adults (y.-adult) and middle-aged (m.-aged).
(F) B16-OVA tumor growth in adult and middle-aged mice treated with vehicle or IL-15 Cx as described in (A), n=7-8/group. Data shown as mean ± SEM with data points representing individual animals. Statistics calculated with MWU test (C,D,F), 2-way ANOVA (E), ns=nonsignificant, *p<0.05, **p<0.01, ***p<0.005.

Early thymic involution in males limits naive CD8 T cell replenishment and facilitates lymph node contraction

Given the significant loss of naive CD8 T cells via memory differentiation and apoptosis, we next asked why this decline is not adequately compensated over time. While no direct causal link has been established between thymic involution and Tvm differentiation, the increased abundance of Tvms in lymphopenic conditions and during aging likely reflects how progressive naive T cell loss makes thymic insufficiency functionally relevant[52–54]. Consistent with published data, we observed thymus involution in humans with significant sex differences, particularly in young adults and middle-aged individuals **(Figure 5A)**, matching the decline in LN size and naive CD8 T cell numbers measured in both mice and humans **(Figure 2E,H)**. Using data from a subsample of the SCAPIS cohort[55], which included thymic health and naïve CD8 T cell counts in middle aged individuals, we showed a significant correlation between poor thymic health and lower numbers of naive CD8 T cells (**Figure 5B**). These observations are corroborated by data from Drabkin *et al.*[56] and the SCAPIS cohort[57] that show age- and sex-related thymus involution using similar CT-based analysis method **(Figure S9A,B,C)**. Across individuals, the thymus involution score and RTE prevalence strongly correlated with the frequency of naive CD8 T cells, linking thymic atrophy to peripheral naive T cell supply **(Figure 5B,C; Figure S9D)**. The sex-biased loss in naive CD8 T cells results from the poorer thymic health in males compared to age-matched females. Interestingly, while CD4 RTEs also declined with age and showed a similar sex bias, naive CD4 T cell numbers remained relatively stable **(Figure S9E)**, consistent with their lower conversion into memory-like cells and increased longevity[40]. In humans, naive CD4 T cell numbers remain relatively stable through midlife, likely due to a compensatory reduction in CD4 T cell loss rate as thymic output wanes[40], whereas naive CD8 T cells exhibit a more pronounced numerical decline and their long-term maintenance appears more variable and less robustly compensated[36,58].

Mechanistically, mouse studies recapitulated these observations. Mimicking the aging effect on LNs with experimental lymphodepletion, naive CD8 T cells recovered faster in middle-aged females than males **(Figure 5D)**. The lymphopenia induced a temporary increase in homeostatic proliferation in LNs that was similar between sexes **(Figure S10A,B).** However, the majority of naive CD8 T cells during recovery was comprised of CD103^{high} recent thymic emigrants (RTEs)[59,60], with a higher prevalence in females **(Figure S10C,D)**. Like in humans, we found significant sex differences in the thymus cellularity of mice **(Figure 5D; Figure S11A-B).** Performing thymectomies (TmX) on young adult mice (**Figure 5E**) significantly reduced RTEs in LNs (detected by signal joint T cell receptor excision circles, sjTREC), eliminated the sex differences found in middle-aged sham surgery treated animals, and abolished the female advantage in LN cellularity and naive CD8 T cell numbers (**Figure 5F,G; Figure S12A**), mirroring the pattern observed in humans, where sex differences are evident when thymic tissue is preserved (score 0–2) but lost upon complete thymic involution (score 3) (**Figure 5B *right***). Interestingly, disrupting the thymus-derived supply of naive T cells by TmX after the initial establishment of the T cell pool increased the relative frequency of Tvm cells in LNs but had no impact on the total Tvm cell counts (**Figure 5J, Figure S12B**). These findings are in line with a model in which Tvm cells, largely established from early-life thymic emigrants[61], persist

independently of thymic output. Their stable numbers after TmX in young adults reflect a tightly regulated balance of naive-to-Tvm conversion, shaped by homeostatic constraints such as IL-15 availability and the transient nature of Tvm residency, as these cells either die or exit the LN, ultimately contributing to LN contraction during aging.

As a result, the loss of naive CD8 T cell replenishment following TmX neutralized sex differences in tumor-specific recognition and CD8 T cell–mediated tumor suppression in middle-aged mice (**Figure 5K-M; Figure S12C,D**), essentially degrading female anti-cancer immune function in middle-age. Collectively, these results demonstrate that the supply of LNs with de novo generated naive CD8 T cells from the thymus remains relevant even later in life in mice and suggest that thymic output continues to contribute to immune maintenance in middle-aged humans, albeit to a progressively lesser extent in males.

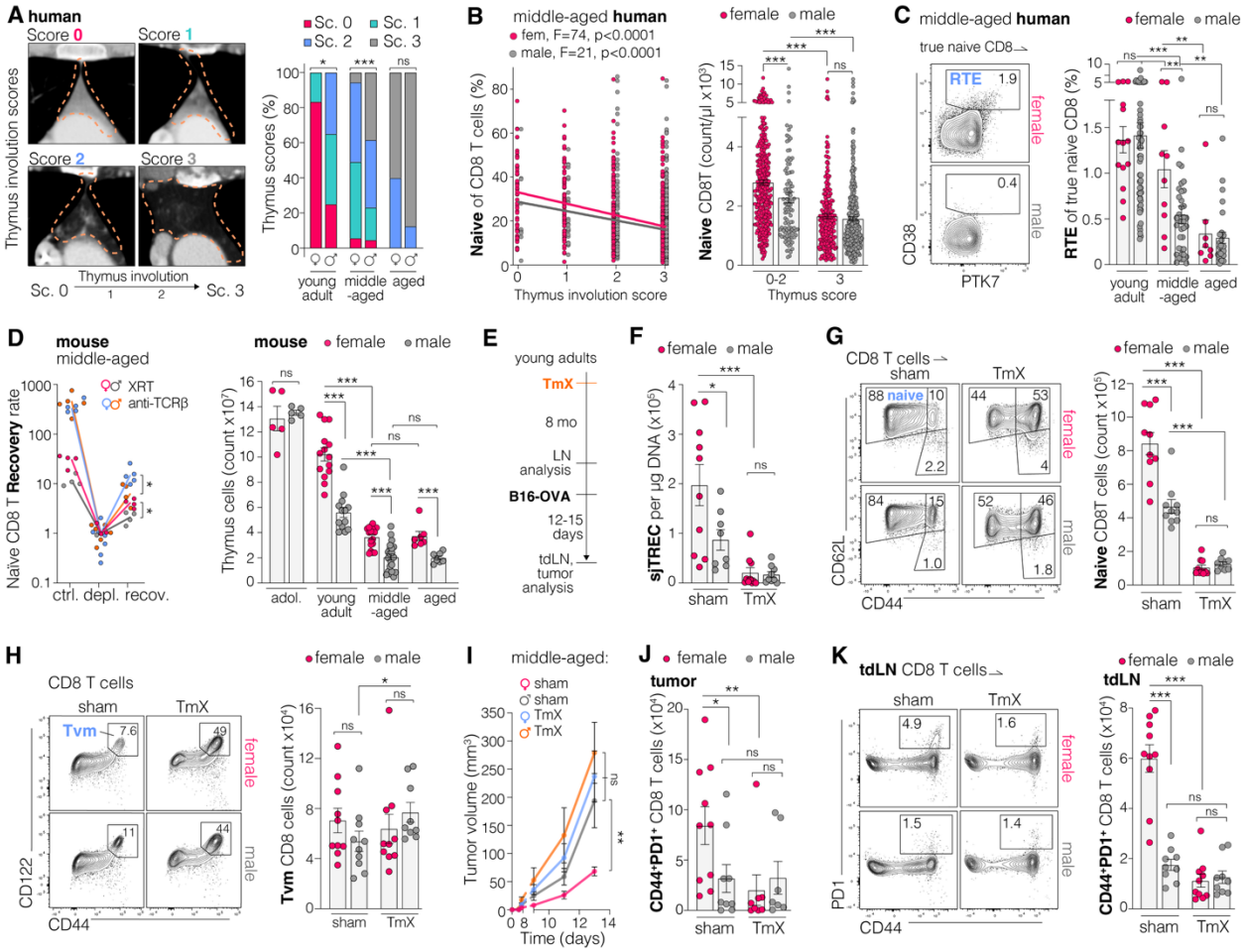

Figure 5. Early thymic involution in males limits naive CD8 T cell replenishment and facilitates LN contraction.
(A) Analysis of human thymus degeneration in CT scans, score (Sc.) 0: predominantly soft tissue; score 1: parity of fatty and soft tissue; score 2: predominantly fat; score 3: complete fatty replacement, Scoring system details in **Figure S11A**.
(B) *Left*, Correlation between the thymus involution score and naive CD8 T cell frequency and *right*, Number of naive CD8 T cells per µl of blood in individuals with preserved thymus (score 0-2) or fully involuted thymus (score 3).
(C) Flow cytometry analysis of human PBMCs for recent thymic emigrants (RTE, CD38^{high}) in true naive CD8 T cells (data

from[8]). Gating strategy in **Figure S5F**.
(D) Recovery rate of naive CD8 T cells 7 days after irradiation (XRT) or anti-TCRß T cell depletion (depl.) and after a period of recovery (recov.) 28 days for XRT and 19 days for anti-TCRß. Cell numbers normalized to average level during depletion.
(E) Experimental set up, thymectomy (TmX) was performed in young mice (5 weeks old), mice were then allowed to age until middle-aged (additional 8 months) and then a LN was analyzed and B16-OVA tumors were implanted.
(F) Signal joint T cell receptor incision cycle (sjTREC) quantification in lymphocytes of LNs from middle-aged mice after sham surgery or TmX performed when young.
(G,H) Flow cytometry of CD8 T cells and quantification of true naive CD8 T cells **(G)** and Tvm **(H)** in middle-aged mice after sham surgery or TmX performed when young. Gating strategy in **Figure S6F**.
(I) B16-OVA tumor growth in middle-aged mice after sham surgery or TmX performed when young, n=9-10/group.
(J,K) Flow cytometry analysis of CD8 T cells from the primary tumor **(J)** or tdLN **(K)**, related to **(I)**.
Data shown as mean ± SEM with data points representing animals or persons. Statistics calculated with MWU test (B,C,D,F,G,H,J,K), Fisher's exact test (A), Pearson correlation (B), 2-way ANOVA (I), ns=nonsignificant, *p<0.05, **p<0.01, ***p<0.005.

Therapeutic thymus regeneration replenishes naive T cells and invigorates tumor-recognition

Thymic atrophy with age results not only from diminished bone marrow–derived lymphoid progenitors and stromal cell senescence, but also from the suppressive effects of sex hormones, particularly androgens[25,62]. While direct evidence is lacking for the extent thymopoiesis in humans can be restored through androgen blockade, clinical data suggest that androgens negatively influences naive CD8 T cell levels[63]. Sex steroid ablation (SSA) is clinically used to treat hormone sensitive prostate cancer – is currently being evaluated in clinical trials, particularly for improving immune regeneration after radiation-induced immunodeficiency[21,64,65]. SSA has shown potential in increasing thymopoiesis and TIL presence in melanoma and advanced prostate cancer[5,66,67]. In mice, SSA partially reverses thymic involution and regenerates the T cell compartment in younger animals, but has minimal effect at advanced age[64,68,69].

To test whether therapeutic SSA could restore naive CD8 T cell availability, improve LN function and finally drive better tumor recognition, we applied both long-term and short-term strategies in mice: surgical gonadectomy (GonX) in early adulthood or middle-aged, and pharmacologic SSA using the FDA approved gonadotropin-releasing hormone antagonist degarelix (DeX) in middle-aged and aged males (**Figure 6A**). Of note, long-term gonadectomy in females (estrogen depletion via ovariectomy) did not significantly alter thymic cellularity, RTE frequency in LNs (sjTREC content), or naive CD8 T cell numbers (**Figure 6B,E,F**). In contrast, both surgical and chemical inhibition approaches for androgens led to increased thymus cellularity and normalized thymocyte development, as reflected by restored double-positive (DP) to double-negative (DN) ratios in males **(Figure 6B,C; Figure S13C,G)**. Importantly, SSA resulted in robust repopulation of LNs, with elevated numbers of RTEs (**Figure 6D,E**). This translated into a significant restoration of naive CD8 T cell numbers in middle-aged males, reaching levels comparable to young adults and untreated middle-aged females. In aged males, DeX treatment also increased naive CD8 T cells, but to a lesser extent, and absolute numbers remained reduced relative to middle-aged mice (**Figure 6F; Figure S13A–M**).

Functionally, these changes eliminated sex-based differences in tumor recognition and response. Following SSA, middle-aged males exhibited increased frequencies of antigen-experienced CD8 T cells in tumor-draining LNs (tdLNs), including $CD44^{+}PD1^{+}$ and $CD39^{+}$ subsets, which mark repeatedly stimulated tumor-reactive T cells. Further, tumor-antigen-specific ($tetramer^{+}$) CD8

tumor-infiltrating lymphocytes (TILs) were also increased, mirroring responses seen in females. Correspondingly, tumor growth dynamics equalized between sexes (**Figure 6G,H; Figure S14A–J**). Preconditioning of middle-aged mice with DeX restored numbers of naive CD8 T cells in LNs and increased the therapeutic response to subsequent anti-PD1 immunotherapy (**Figure 6H *right*; Figure S14K**).

Together, these findings demonstrate that SSA can reinvigorate thymic output, replenish the naive CD8 T cell pool, and enhance antitumor immunity in middle-aged males, thereby eliminating functional sex differences. These data also show that improving naïve CD8 T cell pools in middle aged males can increase responses to anti-PD1 immunotherapy. However, the diminished efficacy of this intervention in aged males highlights the narrowing therapeutic window for immune regeneration in later life.

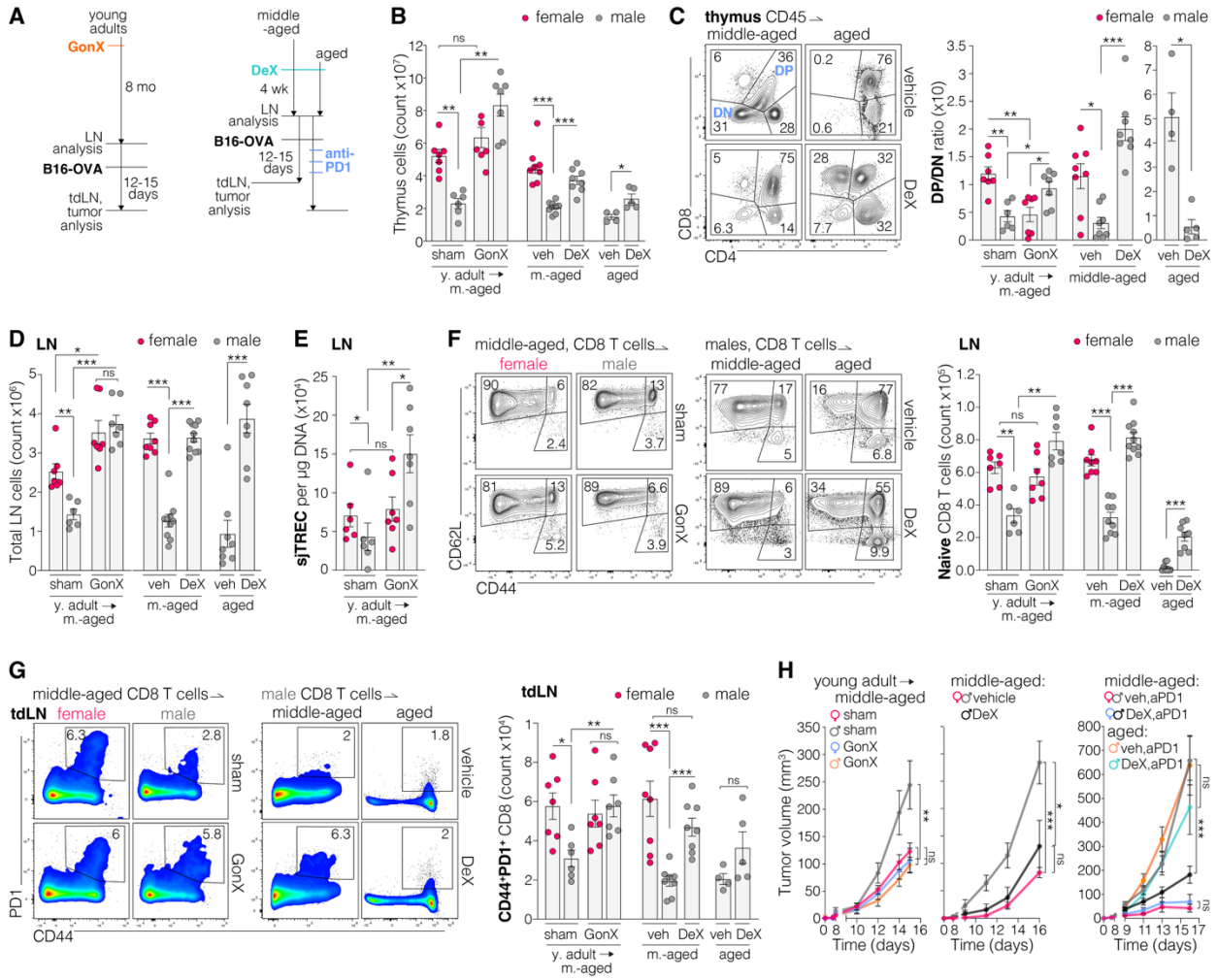

Figure 6. Therapeutic thymus regeneration replenishes naive T cells and invigorates tumor-recognition.
(A) Experimental set up, *left*, young adult and middle-aged mice were gonadectomized (GonX, ovariectomy for females, orchiectomy in males) or, *right*, middle-aged and aged mice were treated with vehicle (veh) or Degarelix (DeX) before analysis of tumor-naive LNs, and implantation and analysis of B16-OVA tumors or treatment with anti-PD1 antibody.
(B) Total count of thymocytes in mice after sham surgery or gonadectomy (GonX) and vehicle (veh) or Degarelix (DeX) treatment in middle-aged and aged mice.

(C) Flow cytometry analysis of thymocytes and double positive (DP) to double negative (DN) ratio. Gating strategy in **Figure S10A**.
(D) Inguinal LN cellularity after treatment as described in **(A)**.
(E) TREC quantification in lymphocytes of LNs after sham surgery or GonX.
(F) Flow cytometry analysis of naive CD8 T cells from ingLNs of mice. Gating strategy in **Figure S6F**.
(G) Flow cytometry analysis of CD8 T cells from tdLNs. Gating strategy in **Figure S3A**.
(H) B16-OVA tumor growth in, *left*, sham and GonX (n=6-7) middle-aged mice, *middle*, vehicle or DeX treated middle-aged mice (n=8/group), and *right*, vehicle or DeX and anti-PD1 treated middle-aged and aged mice (n=7-13/group).
Data shown as mean ± SEM with data points representing individual animals. Statistics calculated with MWU test (B,C,D,E,F,G), 2-way ANOVA (H), ns=nonsignificant, *p<0.05, **p<0.01, ***p<0.005.

Discussion

Our study highlights substantial sex- and age-related disparities in naive CD8 T cell homeostasis and its connection to functional antigen recognition in LNs, illuminating a previously underappreciated link between thymic involution, naive T cell dynamics, and impaired cancer immunity during aging. We demonstrate that males experience an earlier and more profound decline in naive CD8 T cell abundance associated with a contraction of LNs that is critically limiting the repertoire diversity necessary for effective cancer antigen recognition. This deficiency in males results in a skewed intratumoral T cell composition characterized by an increased frequency of antigen-naive bystander T cells and fewer activated tumor-reactive effectors, thereby compromising anti-cancer immunity in middle age. Although T cell infiltration in tumors generally correlates positively with prognosis, the functional status and antigen specificity of tumor-infiltrating lymphocytes (TILs) are paramount determinants of clinical outcomes. Our findings align with reports demonstrating that increased frequencies of naive-like TILs, often associated with age[7], correlate with ineffective anti-cancer responses and poor therapeutic outcomes, highlighting the need for functional rather than numerical assessments of TIL populations in clinical contexts[28,30,31,70]. While aged mice exhibit a significant reduction in T cell receptor (TCR) diversity—up to 80 %—leading to measurable deficits in immune functionality, it remains less clear whether a reduction in T cell clones has equivalent consequences in humans[71–74]. Notably, lymph nodes in aged humans maintain relative clonal diversity[75]. However, our data suggest that a functional TCR repertoire depends not only on the relative diversity but also on the absolute number of unique T cell clones available in draining LNs.

A central insight of our study is the dual mechanisms driving naive CD8 T cell depletion in males: an accelerated antigen-agnostic conversion into Tvm cells compounded by faster loss of thymic function. Prior work has shown total peripheral T cell numbers, which include CD4 T cells, to remain relatively stable with age, largely maintained through homeostatic proliferation and reduced cell loss/increased cellular life span[40]. In line with recent publications[20], our data challenge this paradigm by revealing selective depletion of naive CD8 T cells, particularly driven by premature and excessive differentiation into Tvm cells that cannot be adequately compensated in males due to earlier thymic involution. This sex-biased reduction in naive CD8 T cells profoundly reduces the clonal diversity of the naive T cell pool, critically impairing antigen recognition capacity in tumor-draining LNs. Human data **(Figure 2G,H; Figure 5; Figure S11)** further support this model, showing that while recent thymic emigrants decline in both CD4 and CD8 compartments with age, only naive CD8 T cells undergo a marked numerical reduction. This likely reflects a unique vulnerability of CD8

T cells to antigen-agnostic differentiation into Tvm cells, a process not observed in naive CD4 T cells. One possible contributing factor is the difference in self-antigen presentation: MHC class I molecules continuously present endogenous self-peptides, providing tonic signals that can support Tvm formation in CD8 T cells, whereas MHC class II–restricted self-antigen presentation is more limited, potentially protecting naive CD4 T cells from analogous differentiation.

Of note, other reports highlight thymus-independent CD4 T cell maintenance in humans[11]. CD4 T cells exhibit a lower propensity to lose their naivety through antigen-agnostic memory differentiation in mice[48,76,77] and are less susceptible to phenomena like excessive memory formation, which occurs with CD8 T cells during chronic infections with cytomegalovirus or Epstein-Barr virus in humans[78]. Consequently, while the systemic population of CD4 T cells remains relatively stable over time[40], independent of age and sex, naive CD8 T cells are more prone to Tvm formation, senescence and apoptosis, making maintaining an abundant and diverse repertoire of naive CD8 T cells critically dependent on de novo synthesis in the thymus. Our results support the critical role of thymic output in maintaining naive CD8 T cell populations in adulthood, echoing recent clinical findings linking thymic atrophy with increased cancer risk and mortality in humans[11]. The observed sex disparity in thymic involution during the transition from young adulthood to middle age implies a hormonal influence, with androgens exerting potent inhibitory effects on thymopoiesis[25]. Augmenting lymphoid progenitor cells in the bone marrow by depleting competing myeloid-biased hematopoietic stem cells has shown promise in improving adaptive immune responses but results in only modest increases in naive T cells[22], presumably due to the lack of thymus-based T cell maturation in advanced age. Consistently, therapeutic thymus regeneration via androgen blockade restored naive CD8 T cell numbers, enhanced cancer antigen recognition, and reversed sex-related differences in cancer immunity in middle-aged male mice (**Figure 6,Figure S13** and **Figure S14**). These data underscore the importance of therapeutic interventions targeting thymic regeneration, especially within the defined therapeutic window before advanced age-related changes such as thymus epithelial cell degeneration, LN stromal fibrosis and structural degeneration irreversibly hinder regeneration efforts[14,69,79].

Beyond strategies aimed at enhancing thymic output, interventions mitigating premature Tvm differentiation represent a promising complementary approach. Our demonstration that transient artificial induction of Tvm cells in females recapitulates male-like aging phenotypes in naive T cell compartments strongly suggests that controlling this process could help preserve T cell repertoire diversity independently from hormonal manipulation. Mechanistically, Tvm formation depends on IL-15 availability and the clone-specific TCR affinity for self-antigens[48,53]. Modulating these factors pharmacologically or through lifestyle interventions might provide additional avenues to delay naive T cell depletion and preserve immune competence as males age.

Clinically, our findings have direct implications for improving outcomes of immune checkpoint blockade (ICB) therapies, f which frequently demonstrate limited anti-cancer efficacy due to insufficient tumor-reactive T cell responses[31,80]. Given the central role of naive CD8 T cell availability in generating effective anti-cancer immunity, therapeutic strategies enhancing thymic output or preventing premature naive T cell differentiation may significantly improve clinical responses,

especially in middle-aged and older male populations who experience greater immune impairment. We provide proof-of-concept data to support this strategy. By administering the FDA approved gonadotropin-releasing hormone antagonist degarelix in the neoadjuvant setting to cancer bearing middle-aged male mice, the naïve CD8 T cell pool was expanded and response to anti-PD1 therapy was improved (**Figure 6H**). Our data show that restoring thymic health through androgen depletion can also restore LN health, and with it, anti-cancer immune function. A potential therapeutic strategy to test in the clinic would be neoadjuvant degarelix treatment in middle-aged males prior to immune checkpoint blockade therapy.

Collectively, our study provides compelling evidence for the intertwined roles of thymic functionality and naive T cell dynamics in LNs in shaping sex- and age-specific immune competence. Future research should focus on dissecting molecular pathways governing thymic involution and regeneration, identifying targets for intervention that do not rely solely on hormone ablation, and developing personalized strategies accounting for individual hormonal profiles and age-related immune trajectories. Ultimately, enhancing thymic function and naive T cell maintenance holds significant promise for improving immune responsiveness against cancer and infections, thus promoting healthier aging.

References

1. Haupt, S., Caramia, F., Klein, S. L., Rubin, J. B. & Haupt, Y. Sex disparities matter in cancer development and therapy. *Nat Rev Cancer* **21**, 393–407 (2021).
2. Cook, M. B., McGlynn, K. A., Devesa, S. S., Freedman, N. D. & Anderson, W. F. Sex Disparities in Cancer Mortality and Survival. *Cancer Epidemiol Biomarkers Prev* **20**, 1629–1637 (2011).
3. Yang, C. *et al.* Androgen receptor-mediated CD8+ T cell stemness programs drive sex differences in antitumor immunity. *Immunity* **55**, 1268-1283.e9 (2022).
4. Kwon, H. *et al.* Androgen conspires with the CD8+ T cell exhaustion program and contributes to sex bias in cancer. *Sci Immunol* **7**, eabq2630 (2022).
5. Guan, X. *et al.* Androgen receptor activity in T cells limits checkpoint blockade efficacy. *Nature* **606**, 791–796 (2022).
6. Chhabra, Y. *et al.* Sex-dependent effects in the aged melanoma tumor microenvironment influence invasion and resistance to targeted therapy. *Cell* (2024) doi:10.1016/j.cell.2024.08.013.
7. Georgiev, P. *et al.* Age-associated contraction of tumor-specific T cells impairs antitumor immunity. *Cancer Immunology Research* (2024) doi:10.1158/2326-6066.CIR-24-0463.
8. Chen, A. C. Y. *et al.* The aged tumor microenvironment limits T cell control of cancer. *Nat Immunol* 1–13 (2024) doi:10.1038/s41590-024-01828-7.
9. Mogilenko, D. A. *et al.* Comprehensive Profiling of an Aging Immune System Reveals Clonal GZMK+ CD8+ T Cells as Conserved Hallmark of Inflammaging. *Immunity* **54**, 99-115.e12 (2021).
10. Nikolich-Žugich, J. The twilight of immunity: emerging concepts in aging of the immune system. *Nat Immunol* **19**, 10–19 (2018).
11. den Braber, I. *et al.* Maintenance of Peripheral Naive T Cells Is Sustained by Thymus Output in Mice but Not Humans. *Immunity* **36**, 288–297 (2012).
12. Qi, Q., Zhang, D. W., Weyand, C. M. & Goronzy, J. J. Mechanisms shaping the naïve T cell repertoire in the elderly - thymic involution or peripheral homeostatic proliferation? *Exp Gerontol* **54**, 71–74 (2014).
13. van den Broek, T., Borghans, J. A. M. & van Wijk, F. The full spectrum of human naive T cells. *Nat Rev Immunol* **18**, 363–373 (2018).

14. Kousa, A. I. *et al.* Age-related epithelial defects limit thymic function and regeneration. *Nat Immunol* **25**, 1593–1606 (2024).
15. Sonar, S. A. *et al.* Early age–related atrophy of cutaneous lymph nodes precipitates an early functional decline in skin immunity in mice with aging. *Proc. Natl. Acad. Sci. U.S.A.* **119**, e2121028119 (2022).
16. Mittelbrunn, M. & Kroemer, G. Hallmarks of T cell aging. *Nat Immunol* **22**, 687–698 (2021).
17. Schenkel, J. M. & Pauken, K. E. Localization, tissue biology and T cell state — implications for cancer immunotherapy | Nature Reviews Immunology. *Nature Reviews Immunology* **23**, 807–823 (2023).
18. Sauce, D. *et al.* Evidence of premature immune aging in patients thymectomized during early childhood. *J Clin Invest* **119**, 3070–3078 (2009).
19. Gudmundsdottir, J. *et al.* Early thymectomy leads to premature immunologic ageing: An 18-year follow-up. *Journal of Allergy and Clinical Immunology* **138**, 1439-1443.e10 (2016).
20. Kooshesh, K. A., Foy, B. H., Sykes, D. B., Gustafsson, K. & Scadden, D. T. Health Consequences of Thymus Removal in Adults. *N Engl J Med* **389**, 406–417 (2023).
21. Velardi, E., Tsai, J. J. & van den Brink, M. R. M. T cell regeneration after immunological injury. *Nat Rev Immunol* **21**, 277–291 (2021).
22. Ross, J. B. *et al.* Depleting myeloid-biased haematopoietic stem cells rejuvenates aged immunity. *Nature* **628**, 162–170 (2024).
23. Gustafsson, K. *et al.* *Thymic Mesenchymal Niche Cells Drive T Cell Immune Regeneration*. http://biorxiv.org/lookup/doi/10.1101/2022.10.12.511184 (2022) doi:10.1101/2022.10.12.511184.
24. Al-Habsi, M. *et al.* Spermidine activates mitochondrial trifunctional protein and improves antitumor immunity in mice. *Science* **378**, eabj3510 (2022).
25. Granadier, D., Acenas, D. & Dudakov, J. A. Endogenous thymic regeneration: restoring T cell production following injury. *Nat Rev Immunol* 1–18 (2025) doi:10.1038/s41577-024-01119-0.
26. Durante, M. A. *et al.* Single-cell analysis reveals new evolutionary complexity in uveal melanoma. *Nat Commun* **11**, 496 (2020).
27. Sade-Feldman, M. *et al.* Defining T Cell States Associated with Response to Checkpoint Immunotherapy in Melanoma. *Cell* **175**, 998-1013.e20 (2018).
28. Li, H. *et al.* Dysfunctional CD8 T Cells Form a Proliferative, Dynamically Regulated Compartment within Human Melanoma. *Cell* **176**, 775-789.e18 (2019).
29. Zhang, C. *et al.* A single-cell analysis reveals tumor heterogeneity and immune environment of acral melanoma. *Nat Commun* **13**, 7250 (2022).
30. Meier, S. L., Satpathy, A. T. & Wells, D. K. Bystander T cells in cancer immunology and therapy. *Nat Cancer* **3**, 143–155 (2022).
31. Scheper, W. *et al.* Low and variable tumor reactivity of the intratumoral TCR repertoire in human cancers. *Nat Med* **25**, 89–94 (2019).
32. De Togni, P. *et al.* Abnormal development of peripheral lymphoid organs in mice deficient in lymphotoxin. *Science* **264**, 703–707 (1994).
33. Chi, L. *et al.* Sexual dimorphism in skin immunity is mediated by an androgen-ILC2-dendritic cell axis. *Science* **384**, eadk6200 (2024).
34. Bekkhus, T., Olofsson, A., Sun, Y., Magnusson, P. U. & Ulvmar, M. H. Stromal transdifferentiation drives lipomatosis and induces extensive vascular remodeling in the aging human lymph node. *The Journal of Pathology* **259**, 236–253 (2023).
35. Hale, B. D. *et al.* Cellular architecture shapes the naïve T cell response. *Science* **384**, eadh8697 (2024).
36. Terekhova, M. *et al.* Single-cell atlas of healthy human blood unveils age-related loss of NKG2C+GZMB−CD8+ memory T cells and accumulation of type 2 memory T cells. *Immunity* **56**, 2836-2854.e9 (2023).
37. Bohacova, P. *et al.* Multidimensional profiling of human T cells reveals high CD38 expression, marking recent thymic emigrants and age-related naive T cell remodeling. *Immunity* **0**, (2024).
38. Domínguez Conde, C. *et al.* Cross-tissue immune cell analysis reveals tissue-specific features in humans. *Science* **376**, eabl5197 (2022).
39. Ashouri, J. F. & Weiss, A. Endogenous Nur77 Is a Specific Indicator of Antigen Receptor Signaling in Human T and B Cells. *The Journal of Immunology* **198**, 657–668 (2017).

40. Mold, J. E. *et al.* Cell generation dynamics underlying naive T-cell homeostasis in adult humans. *PLoS Biol* **17**, e3000383 (2019).
41. Goronzy, J. J. & Weyand, C. M. Mechanisms underlying T cell ageing. *Nat Rev Immunol* **19**, 573–583 (2019).
42. Quinn, K. M. *et al.* Age-Related Decline in Primary CD8+ T Cell Responses Is Associated with the Development of Senescence in Virtual Memory CD8+ T Cells. *Cell Rep* **23**, 3512–3524 (2018).
43. Chiu, B.-C., Martin, B. E., Stolberg, V. R. & Chensue, S. W. Cutting Edge: Central Memory CD8 T Cells in Aged Mice Are Virtual Memory Cells. *The Journal of Immunology* **191**, 5793–5796 (2013).
44. Pulko, V. *et al.* Human memory T cells with a naïve phenotype accumulate with aging and respond to persistent viruses. *Nat Immunol* **17**, 966–975 (2016).
45. Azzam, H. S. *et al.* CD5 expression is developmentally regulated by T cell receptor (TCR) signals and TCR avidity. *J Exp Med* **188**, 2301–2311 (1998).
46. Wong, P., Barton, G. M., Forbush, K. A. & Rudensky, A. Y. Dynamic tuning of T cell reactivity by self-peptide-major histocompatibility complex ligands. *J Exp Med* **193**, 1179–1187 (2001).
47. Drobek, A. *et al.* Strong homeostatic TCR signals induce formation of self-tolerant virtual memory CD8 T cells. *The EMBO Journal* **37**, e98518 (2018).
48. White, J. T. *et al.* Virtual memory T cells develop and mediate bystander protective immunity in an IL-15-dependent manner. *Nat Commun* **7**, 11291 (2016).
49. Park, J.-E. *et al.* A cell atlas of human thymic development defines T cell repertoire formation. *Science* **367**, eaay3224 (2020).
50. Cordes, M. *et al.* Single-cell immune profiling reveals thymus-seeding populations, T cell commitment, and multilineage development in the human thymus. *Science Immunology* **7**, eade0182 (2022).
51. Moskowitz, D. M. *et al.* Epigenomics of human CD8 T cell differentiation and aging. *Sci. Immunol.* **2**, eaag0192 (2017).
52. Akue, A. D., Lee, J.-Y. & Jameson, S. C. Derivation and Maintenance of Virtual Memory CD8 T Cells. *The Journal of Immunology* **188**, 2516–2523 (2012).
53. White, J. T., Cross, E. W. & Kedl, R. M. Antigen-inexperienced memory CD8+ T cells: where they come from and why we need them. *Nat Rev Immunol* **17**, 391–400 (2017).
54. Min, B. *et al.* Neonates support lymphopenia-induced proliferation. *Immunity* **18**, 131–140 (2003).
55. Bergström, G. *et al.* The Swedish CArdioPulmonary BioImage Study: objectives and design. *J Intern Med* **278**, 645–659 (2015).
56. Drabkin, M. J. *et al.* Age-stratified Patterns of Thymic Involution on Multidetector CT. *Journal of Thoracic Imaging* **33**, 409–416 (2018).
57. Sandstedt, M. *et al.* Complete fatty degeneration of thymus associates with male sex, obesity and loss of circulating naïve CD8+ T cells in a Swedish middle-aged population. *Immun Ageing* **20**, 45 (2023).
58. Thomson, Z. *et al.* Trimodal single-cell profiling reveals a novel pediatric CD8αα+ T cell subset and broad age-related molecular reprogramming across the T cell compartment. *Nat Immunol* (2023) doi:10.1038/s41590-023-01641-8.
59. Staton, T. L., Johnston, B., Butcher, E. C. & Campbell, D. J. Murine CD8+ Recent Thymic Emigrants are αE Integrin-Positive and CC Chemokine Ligand 25 Responsive1. *The Journal of Immunology* **172**, 7282–7288 (2004).
60. McFarland, R. D., Douek, D. C., Koup, R. A. & Picker, L. J. Identification of a human recent thymic emigrant phenotype. *Proceedings of the National Academy of Sciences* **97**, 4215–4220 (2000).
61. Smith, N. L. *et al.* Developmental Origin Governs CD8+ T Cell Fate Decisions during Infection. *Cell* **174**, 117-130.e14 (2018).
62. Taves, M. D. & Ashwell, J. D. Effects of sex steroids on thymic epithelium and thymocyte development. *Front. Immunol.* **13**, (2022).
63. Lakshmikanth, T. *et al.* Immune system adaptation during gender-affirming testosterone treatment. *Nature* **633**, 155–164 (2024).
64. Sutherland, J. S. *et al.* Activation of Thymic Regeneration in Mice and Humans following Androgen Blockade. *The Journal of Immunology* **175**, 2741–2753 (2005).
65. Sutherland, J. S. *et al.* Enhanced Immune System Regeneration in Humans Following Allogeneic or Autologous Hemopoietic Stem Cell Transplantation by Temporary Sex Steroid Blockade. *Clinical Cancer Research* **14**, 1138–1149 (2008).

66. Robert, C. *et al*. Phase I Study of Androgen Deprivation Therapy in Combination with Anti–PD-1 in Melanoma Patients Pretreated with Anti–PD-1. *Clinical Cancer Research* **29**, 858–865 (2023).
67. Morse, M. D. & McNeel, D. G. Prostate Cancer Patients Treated with Androgen Deprivation Therapy Develop Persistent Changes in Adaptive Immune Responses. *Hum Immunol* **71**, 496–504 (2010).
68. Heng, T. S. P. *et al*. Impact of Sex Steroid Ablation on Viral, Tumour and Vaccine Responses in Aged Mice. *PLoS ONE* **7**, e42677 (2012).
69. Thompson, H. L. *et al*. Lymph nodes as barriers to T-cell rejuvenation in aging mice and nonhuman primates. *Aging Cell* **18**, e12865 (2019).
70. Simoni, Y. *et al*. Bystander CD8+ T cells are abundant and phenotypically distinct in human tumour infiltrates. *Nature* **557**, 575–579 (2018).
71. Nanda, N. K., Apple, R. & Sercarz, E. Limitations in plasticity of the T-cell receptor repertoire. *Proc Natl Acad Sci U S A* **88**, 9503–9507 (1991).
72. Blackman, M. A. & Woodland, D. L. The narrowing of the CD8 T cell repertoire in old age. *Current Opinion in Immunology* **23**, 537–542 (2011).
73. Woodland, D. L., Kotzin, B. L. & Palmer, E. Functional consequences of a T cell receptor D beta 2 and J beta 2 gene segment deletion. *J Immunol* **144**, 379–385 (1990).
74. Qi, Q. *et al*. Diversity and clonal selection in the human T-cell repertoire. *Proc. Natl. Acad. Sci. U.S.A.* **111**, 13139–13144 (2014).
75. Thome, J. J. C. *et al*. Long-term maintenance of human naïve T cells through in situ homeostasis in lymphoid tissue sites. *SCIENCE IMMUNOLOGY* (2016).
76. Sosinowski, T. *et al*. CD8α+ Dendritic Cell Trans Presentation of IL-15 to Naive CD8+ T Cells Produces Antigen-Inexperienced T Cells in the Periphery with Memory Phenotype and Function. *The Journal of Immunology* **190**, 1936–1947 (2013).
77. Moon, J. J. *et al*. Naive CD4+ T Cell Frequency Varies for Different Epitopes and Predicts Repertoire Diversity and Response Magnitude. *Immunity* **27**, 203–213 (2007).
78. Almanzar, G. *et al*. Long-Term Cytomegalovirus Infection Leads to Significant Changes in the Composition of the CD8+ T-Cell Repertoire, Which May Be the Basis for an Imbalance in the Cytokine Production Profile in Elderly Persons. *Journal of Virology* **79**, 3675–3683 (2005).
79. Masters, A. R. *et al*. Assessment of Lymph Node Stromal Cells as an Underlying Factor in Age-Related Immune Impairment. *J Gerontol A Biol Sci Med Sci* **74**, 1734–1743 (2019).
80. Miller, J. F. A. P. The function of the thymus and its impact on modern medicine. *Science* **369**, eaba2429 (2020).
81. Roth, H. R. *et al*. A New 2.5D Representation for Lymph Node Detection using Random Sets of Deep Convolutional Neural Network Observations. *Med Image Comput Comput Assist Interv* **17**, 520–527 (2014).
82. Rister, B., Shivakumar, K., Nobashi, T., & Rubin, D. L. CT-ORG: ADataset of CT volumes with multiple organ segmentations. *The Cancer Imaging Archive (TCIA)* 10.7937/tcia.2019.tt7f4v7o (2019).
83. Zhou, H. *et al*. Cancer immunotherapy response persists after lymph node resection. 2023.09.19.558262 Preprint at https://doi.org/10.1101/2023.09.19.558262 (2024).
84. McFarlane, L., Truong, V., Palmer, J. S. & Wilhelm, D. Novel PCR assay for determining the genetic sex of mice. *Sex Dev* **7**, 207–211 (2013).
85. Borcherding, N., Bormann, N. L. & Kraus, G. scRepertoire: An R-based toolkit for single-cell immune receptor analysis. *F1000Res* **9**, 47 (2020).

Acknowledgments

We thank Dr. Peigen Huang and the Cox-7 animal facility for maintaining and providing mice and technical support; Mark Duquette for providing help and technical assistance. We thank Dr. Marina Terekhova, Dr. Pavla Bohacova and the lab of Dr. Maxim N. Artyomov for granting access to data sets of human PBMCs. The results shown in Figure S1A are in whole or part based upon data generated by the TCGA Research Network: https://www.cancer.gov/tcga. We thank the NIH Tetramer Core Facility (contract number 75N93020D00005) for providing tetramers for flow cytometry.

Data and code availability

All data are available in the main text or the supplementary materials.

Author contributions

Conceptualization: LM, TPP; methodology: LM, TPP, DRS, MZ, LLM; investigation: LM, MZ, MJO, HZ, LL, PL, MS, LJ; visualization: LM, LLM; Supervision: TPP, DRS; writing the original draft: LM, TPP; review & editing: LM, TPP

Competing interests

The authors declare no competing financial interests. Co-author Hengbo Zhou is now employed by Arnatar Therapeutics; his affiliation with Arnatar began after completion of the work presented here, and there is no connection between Arnatar and the present study.

Funding

German Research Foundation grant ME 5486/1-2 (LM)

National Institutes of Health grant F32CA275298 (MJO)

National Institutes of Health grant K00CA234940 (HZ)

National Institutes of Health grant R21AG072205 (TPP)

National Institutes of Health grant R01CA214913 (TPP)

National Institutes of Health grant R01HL128168 (TPP)

National Institutes of Health grant R01CA284372 (TPP)

National Institutes of Health grant R01CA284603 (TPP, LLM)

The Rullo Family MGH Research Scholar Award (TPP)

Melanoma Research Alliance (DRS)

V Foundation for Cancer Research (DRS)

NIAID DP2 AI176139 (DRS)

NIAID U19 AI082630 (DRS)

Heart–Lung Foundation, Sweden (20180436)

Swedish Research Council (2018–03232)

Materials and Methods

Mice

Wild type C57BL/6 mice, *Lta*$^{-/-}$ (lymphotoxin alpha knockout mice B6.129s2-Ltatm1Dch/J from the Jackson Laboratory, Strain# 002258) and OT-1 (C57BL/6-Tg(TcraTcrb)1100Mjb/J) were used for animal models. All mice were bred and maintained at in animal facilities of the Massachusetts General Hospital with housing in accordance with procedures outlined in the National Institutes of Health's Guide for the Care and Use of Laboratory Animals. Mice received a standard pelleted rodent diet and tap water ad libitum and were maintained at 20-24°C, 70 % humidity and 12/12-hour light/dark cycle. All experiments were performed at the Massachusetts General Hospital (MGH) and approved by the Institutional Animal Care and Use Committee (IACUC) of the MGH under the protocol numbers 2023N000101, 2011N000085 and 2004N000123. Age- and sex-matched groups of adolescents (4-5 weeks), young adults (7-10 weeks), middle-aged (9-12 month) and aged (>18 month-old) female and male mice were used in each experiment unless specified otherwise.

Animal models and tumor cell lines

The B16F10 melanoma cell line (ATCC) was cultured according to the supplier's recommendations. B16F10-OVA cells were a gift from Dr. Susan Thomas, Georgia Institute of Technology. B16F10-SIINFEKL-zsGreen cells were generated in-house as described previously[83]. All cell lines were regularly tested for mycoplasma. For tumor engraftment, B16F10 or B16-OVA cells (5×10^5) were injected intradermally into the lower flank of mice. Animals were monitored daily, and tumor volumes were measured every 2–3 days. Tumor volume was calculated as: tumor volume = width × length × (width/2). For survival analyses, animals were euthanized based on approved humane endpoints once the tumor exceeded 1,000 mm^3 or reached 2 cm in any diameter.

Study population

The Swedish CArdioPulmonary bioImage Study (SCAPIS) is a general population-based prospective study[55]. Middle-aged participants (50–64 years old females and males) underwent comprehensive clinical examination including imaging and functional studies of the heart and lungs, covering the thymus, and completed extensive questionnaires to assess lifestyle, post and current medication regiments. Blood samples from a subsample, SCAPIS Leukocyte (n=1078), were taken to profile immune cell compositions in fresh whole blood. Among the participants in SCAPIS Leukocyte, assessments of thymus were also performed on computed tomography (CT) scans. Twenty-nine participants (2.7%) were excluded from analysis: 9 (0.8%) due to missing images, 6 (0.6%) with anterior mediastinal lymphadenopathy or tumor, 5 (0.5%) with prior surgery preventing evaluation, 2 (0.2%) with imaging artefacts, and 7 (0.6%) for miscellaneous anatomical or technical reasons.

Volume segmentation in CT scans

Computed tomography (CT) scans of human individuals are from the Cancer Imaging Archive of the National Institutes of Health (NIH)[81,82] and were analyzed using 3D Slicer (version 5.6.2).

Lymph node (LN) analysis: Body scans were cropped to the axillary or inguinal regions. Superficial skin areas were excluded. The segmentation threshold was adjusted to include LNs while excluding

surrounding fatty tissue and skin. Using 3D volume rendering, LNs were identified and surrounding tissues removed manually until only individual LNs remained. The average LN volume per individual was used for statistical analysis. Datasets with one or more pathologically enlarged LNs (>700 mm^3) were excluded.

Spleen analysis**:** Scans were cropped to the region beneath the lungs to isolate the spleen. The segmentation threshold was adjusted to include the spleen while excluding surrounding fatty tissue. 3D volume rendering was used to identify the spleen and manually remove extraneous tissue.

Thorax analysis**:** Scans were cropped between the clavicles and the upper pelvis. The segmentation threshold was set to include all tissue within the thorax. Using 3D volume rendering, objects not part of the human thorax (e.g., scanning table) were removed.

Thymus analysis: scans were assessed as described[57]. In brief, thymus fat and soft tissue content was visually analyzed and graded on a scale 0–3, grade score 0: predominantly soft tissue, score 1: parity of fatty and soft tissue; score 2: predominantly fat; score 3: complete fatty replacement **(Figure S11a)**.

Thymus analysis of the SCAPIS cohort: CT scans of the thorax was performed along the guidelines of the SCAPIS protocols[55]. All scans were reviewed using a fixed window setting and evaluated by an experienced thoracic radiologist[57].

Organ resection procedures

LN dissection: A 0.5 cm skin incision exposed the inguinal LN. Vessels were compressed with fine curved forceps, and the LN was excised. The skin was closed with wound clips, and mice recovered for ≥14 days.

Splenectomy: The spleen was accessed via an incision through the skin and peritoneum at the right flank. Vascular connections at the splenic hilum were ligated, and the spleen was removed. The peritoneum and skin were closed, and mice recovered for ≥14 days.

Thymectomy: Thymectomies were performed on 6-week-old mice. A semicircular skin incision along the upper thorax and a sternal incision were made to expose and remove both thymic lobes. The chest was closed with sutures and skin with wound clips. Mice were allowed to mature to middle age. Complete removal and absence of thymic regeneration were verified visually during surgery and at experiment end.

Orchiectomy: The testis, epididymis, and fat pad were gently exteriorized via a small scrotal incision. A ligature was placed below the testis and epididymis, which were then removed. The scrotal incision was sutured, and mice recovered for ≥14 days.

Ovariectomy: Ovaries were accessed through a midline incision along the back. A ligature was placed at the oviduct-uterus boundary, and the ovaries were excised. The peritoneum was sutured, skin closed with wound clips, and mice recovered for ≥14 days.

Chemical sex steroid ablation

Degarelix (MedChemExpress) was dissolved in a solution of 10% DMSO, 40% PEG3000, 5% Tween-80, and 45% saline. It was administered subcutaneously at 0.25 mg once weekly for four consecutive weeks. Control mice received vehicle only.

In vivo treatments

Mice were injected intraperitoneally with immune-modulating antibodies or cytokine complexes. For PD-1 blockade, anti-PD-1 mAb (clone RMP1-14, Bio X Cell) was administered at 10 mg/kg three times every 3 days. For T cell depletion, anti-TCRβ mAb (clone H57-597, Bio X Cell) was given at 10 mg/kg once. For CD8 T cell depletion, anti-CD8α mAb (clone 53-6.7, Bio X Cell) was administered at 10 mg/kg, four times every 5 days. For IL-15/IL-15Rα complex (IL-15 Cx) treatment, IL-15 Cx (6 µg, Sino Biological) or vehicle (0.9 % SoCl solution) were administered four times once per week.

Immunization of mice

Tumor cell lysates were prepared by subjecting 1×10^8 cells/mL in sterile water to five freeze-thaw cycles (liquid nitrogen and 37°C water). Fifty microliters of tumor cell lysate or DQ-OVA solution (Invitrogen) containing 10 µg of LPS as adjuvant, or PR8 virus particles (1×10^5 inactivated particles with 2 µg poly(I:C) and 2 µg anti-CD40 mAb [clone MR-1, Bio X Cell]) or respective controls were injected intradermally into the lower flank. Draining inguinal LNs and the contralateral inguinal (non-draining) LNs were analyzed 24- or 72-hours post-immunization.

Tissue Dissection and single-cell preparation

Mice were euthanized, and tissues were resected and mechanically dissociated. Single-cell suspensions from the thymus were filtered through a 40 µm strainer. Single-cell suspensions from tumor and spleen were filtered through a 70 µm strainer. Individual LNs were mechanically dissociated by gently pressing them with a syringe plunger against the surface of a sterile petri dish. Cells in the resulting suspension were counted before any filtering or centrifugation to ensure reliable cell counts without technical artifacts. For flow cytometry analysis of antigen presenting cells, LNs were treated with 1 mg/ml Collagenase-D (Sigma) and 0.1 mg/ml DNAse-I (Roche, in HBSS) for 30 min at 37°C before mechanical dissociation. Blood and spleen samples underwent hemolysis with ACK buffer (Thermo Fisher Scientific).

Flow cytometry

Single-cell suspensions were incubated with LIVE/DEAD Zombie dye (BioLegend) and anti-mouse CD16/32 in PBS for 15 min at 4°C to block Fc receptors and stain for viability. When applicable, tetramers were added for 1 hour at room temperature. Surface staining was then performed with fluorochrome-conjugated antibodies in flow buffer (2% FCS, 0.5 mM EDTA in PBS) for 20 min at room temperature (antibody list in **Table S1**). After washing, cells were fixed and permeabilized using the Foxp3/Transcription Factor Staining Set (eBioscience) for 30–60 min at 4°C, followed by intracellular staining for ≥1 hour at 4°C. Data were acquired using an Aurora spectral flow cytometer (Cytek) and analyzed with FlowJo (v.10.1, TreeStar).

Immunohistochemistry

Tissues were fixed in 4% PFA at 4°C overnight (ON) and incubated in 30% sucrose ON at 4°C. Samples were embedded in OCT compound (Tissue-tek), frozen, and cryosectioned (10 µm). Sections were washed in PBS, blocked (5% donkey serum, 0.25% Triton X-100 in PBS) for 1 h at room temperature, and incubated with primary antibodies overnight at 4°C. After washing, sections were

incubated with secondary antibodies (Jackson ImmunoResearch), counterstained with DAPI, and mounted in Vectashield (Vector Laboratories). Images were acquired using an AxioScan Z.1 microscope (Zeiss) and analyzed with ImageJ.

Enzyme-linked immunoassay

Serum ***testosterone*** levels were measured using a testosterone ELISA kit (Crystal Chem) following the manufacturer's instructions. For ***IL-15/IL-15Rα complex*** (IL-15 Cx) measurements, individual inguinal LNs were weighed and homogenized in 100 µL RIPA buffer. Fifty microliters of lysate per sample were used for ELISA (Thermo Fisher Scientific) according to the manufacturer's protocol.

PCR to determine sex from genomic DNA

Genetic sex of tumor cell lines was determined as described[84]. DNA was extracted (DNA extraction columns from Zymo Research) from cultured tumor cells (B16F10, female controls: 4T1, Yumm3.3) or male splenocytes. PCR was performed using primer pairs listed in **Table S2** with Hot Start Taq Plus polymerase (Qiagen). Parameters: 95°C for 2 min, 35 cycles with 94°C for 30 s, 56°C (*SX* and *Ube* primers) and 55°C (*Zfy* primers) for 30 s, and 72°C for 30 s, followed by final elongation at 72°C for 5 min. PCR products were resolved on 2% agarose gels and visualized with GelRed (Biotium).

sjTREC PCR detection in mice

Genomic DNA from LN cells was extracted using the DNeasy Blood & Tissue Kit (Zymo Research) per the manufacturer's instructions. qPCR with primers and probe specific for single joint T cell receptor excision circles (sjTREC, **Table S2**) was performed using PrimeTime™ Gene Expression Master Mix (IDT). Parameters: 95°C for 5 min, 45 cycles with 95°C for 30 s, 60°C for 30 s, and 60°C for 30 s, followed by final elongation at 72°C for 5 min. Standard curves were generated using a plasmid containing the sjTREC sequence (gift from Karin Gustafson, MGH). sjTREC copy number per µg DNA was calculated from the standard curve.

TREC PCR detection in humans

Peripheral blood mononuclear cells were isolated using Ficoll gradient centrifugation, DNA purification using QIAamp DNA Mini Kit (Qiagen). Levels of TRECs were analyzed with droplet digital PCR (BioRad) using primer pairs listed in **Table S2** and a reaction mix consisting of Supermix (ddPCR BioRad) and Hind III reaction enzyme (BioNordika) together with 1.1 µg DNA per reaction. An automatic droplet generator (QX200 Droplet Generator, BioRad) was used followed by PCR amplification (C1000 Touch Thermal Cycler, BioRad). Results were presented as copies/µL. A sample from a 29 years old healthy young adult was used as positive control and a no template control was included in each run.

TCR sequencing

CD8 T cells were isolated from individual inguinal LNs using the EasySep™ Mouse CD8 T Cell Isolation Kit (StemCell Technologies). Sorted cells were submitted to iRepertoire for TCR sequencing and bioinformatic analysis. This included RNA isolation, reverse transcription, amplification of *TRA* and *TRB* CDR3 regions, and sequencing to assess T cell clonality and diversity.

Shannon entropy

Shannon entropy was calculated to determine TCR diversity. The frequency of each clonotype was used to compute probabilities (p_i = frequency_i/N_total), and entropy (H) was calculated as:

$$H = -\sum_{i=1}^{N} p_i \log_2 p_i$$

where N is the total number of unique clonotypes.

Shannon entropy approximations: The average values of total TRB and unique TRB of all 6 samples (3 female, 3 male) were used to calculate theoretical values of samples with similar characteristics and a certain diversity (100 % and 50 % unique TCRs). Entropy was computed using the formula (described below). Probabilities for unique clonotypes were calculated as $p_{unique}=1/N_{total}$, while probabilities for expanded clonotypes were based on their observed frequencies. The total entropy was obtained by summing the contributions from unique and expanded clonotypes.

(Case **A**, 100 %) maximum diversity means each sequence is unique and appears exactly once, calculation with $H=\log_2 N$;

(Case **B**, 50 % with a single highly expanded clonotype):

$H_{unique}=-N_{unique}\times p_{unique}\times \log_2 p_{unique}$

equation for expanded clonotypes: $H_{expanded}=-p_{expanded}\times \log_2 p_{expanded}$

equation for combined entropy: $H_{total}=H_{unique}+H_{expanded}$

(Case **C**, 50 % duplicates evenly distribution among 10 expanded clonotypes):

$N_{expanded}=N_{unique}/10$

$P_{expanded}=N_{expanded}/N_{total}$

$H_{unique}=-N_{unique}\times p_{unique}\times \log_2 p_{unique}$

$H_{expanded}=-10 \times p_{expanded}\times \log_2 p_{expanded}$

$H_{total}=H_{unique}+H_{expanded}$

Re-analysis of spectral flow data

Spectral flow data from Bohacova *et al.*[37] (Synapse: syn53238646) were analyzed using the gating strategy as described in **Figure S5F** with the aim to quantify true naive CD8 and CD4 cells and with an emphasis to exclude all non-true naive T cells that might interfere with the subsequent quantification of recent thymic emigrants (RTEs)[37]. The following markers were used in **live cells**: $CXCR5^-/CD19^-$ (exclude B cells, T follicular helper cells), $CD14^-/CD123^-$ (exclude myeloid cells), $NKp80^-/CD56^-$ (exclude NK cells), TCR γ/ $\delta^-/CD3^+$ (exclude γ/δ T cells, include all other T cells), gating on **CD8 T cells**: $CD25^-/PD1^-/FAS^-/GZMB^-$ (exclude cells expressing activation markers), CD27+/CD45RA+ (true naive CD8 T cells), $CD38^{high}$ (RTE). **CD4 T cells**: $FAS^-/CXCR3^-$ (exclude cells expressing activation markers), $CD127^+/CD25^-$ (excluding regulatory T cells), $CD27^+/CD45RA^+$ (true naive CD8 T cells), $CD38^{high}$ (RTE). Data were analyzed with FlowJo (v.10.1, TreeStar).

Re-analysis of scRNA-seq data

All scRNA-seq data were analyzed with Seurat (v.5).

Human PBMC public scRNA-seq data[36] from Terekhova et al.[36] Synapse: syn49637038, were filtered for CD8 T cells and assigned a "*naive score*" using the Ucell package with positive and negative modulator genes (*LEF1*$^+$*, TCF7*$^+$*, KLF2*$^+$*, BACH2*$^+$*, FOXP1*$^+$*, GZMB*$^-$*, PRDM1*$^-$*, TBX21*$^-$*, FAS*$^-$*, EOMES*$^-$).
H*uman LN cells* from public scRNA-seq data[38], were filtered for CD8 T cells and assigned a "*naive score*" as described above. Antigen presenting cells (APCs) from the same data set were analyzed using the cell subset attribution from the original publication. scTCR-seq data of T cells from LNs of the same data set were analyzed using the scRepertoire[85] (v.2.3.0) package in R.
Human melanoma data sets from Durante *et el.*[26] GSE139829; Sade-Feldman *et al.* [27] GSE120575; Li et al.[28] GSE123139; Zhang et al.[29] GSE215121). Cells of individual patients were filtered for CD8 T cells and percentage of naive, cytotoxic and exhausted attributed with module scores using the Ucell package (naive: *SELL, CCR7*; cytotoxic: *GZMA, GZMB, PRF1, IFNG, PTPN6, GNLY*; exhausted: *HAVCR2, TOX, TIGIT*.
Human thymocyte public scRNA-seq data from Park et al.[49] (https://zenodo.org/records/3711134) and Cordes et al.[50] GSE195812, were assigned for subsets using the Ucell package with positive and negative modulator genes (double negative (DN)1: *CD34*$^+$*, HES1*$^+$*, IL7R*$^+$*, TRAC*$^-$*;* DN2: *HES1*$^+$*, PTCRA*$^+$*, TRAC*$^-$; *DN3: NOTC1*$^+$*, PTCRA*$^+$*, CD8A*$^-$*, CD4*$^-$*;* DN4: *RAG1*$^+$*, BCL11B*$^+$*, PTCRA*$^+$*, CD8A*$^-$*, CD4*$^-$; double positive (DP): *RAG1*$^+$*, CD8A*$^-$*, CD4*$^-$; single positive (SP) CD8: *CD8A*$^+$*, CD8B*$^+$*, TRAC*$^+$*, CD4*$^-$; SP CD4: *TRAC*$^+$*, CD4*$^+$; Treg: *FOXP3*$^+$*, IL2RA*$^+$*, IKZF2*$^+$; mature naive: *CCR7*$^+$*, TRAC*$^+$*, FOXP1*$^+$*, KLF2*$^+$*, CD8A*$^+$*, CD4*$^+$; *CD69*$^-$, *IL2RA*$^-$, γδ T cells: *TRDC*$^+$*, SOX13*$^+$*, TRAC*$^-$; *CD8A*$^-$, *CD8B*$^-$, *CD4*$^-$.

Immune scores

Immune scores were derived from transcriptomic data of melanoma tumors from The Cancer Genome Atlas (TCGA) using the ESTIMATE (Estimation of Stromal and Immune cells in Malignant Tumor tissues using Expression data) platform developed at MD Anderson Cancer Center, University of Texas.

Statistical analysis

Groups were compared using Prism software (GraphPad, v.10). The statistical methods used are described in the figure legends and include Mann-Whitney U test (MWU), independent-sample t test, log-rank test, 2-way ANOVA, Fisher's exact test and Pearson correlation. In the SCAPIS data, a sex effect controlling for age was evaluated using General Linear Model (GLM). Statistical significance is indicated in figures as ns=nonsignificant, *$p<0.05$, **$p<0.01$, ***$p<0.005$.

Supplemental figures

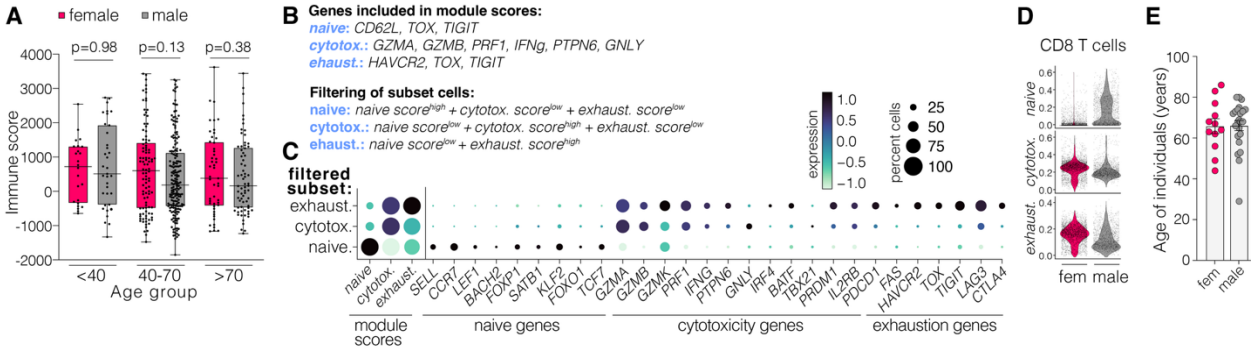

Figure S1. T cell infiltration in melanoma.
(A) Immune scores derived from The Cancer Genome Atlas (TCGA) transcriptomic data of melanoma samples, indicating tumor infiltration of T cells.
(B) Genes that are included in the module scores and use of module score combinations to identify CD8 T cell subsets in tumors.
(C) Module score levels and expression levels of canonical marker genes shown for filtered subsets. Integrated data from Durante *et al.*[26], Sade-Feldman *et al.*[27], Li *et al.*[28], Zhang *et al.*
(D) Module score expression data of CD8 T cells from Durante *et al.*[26]
(E) Age of melanoma patients (when available, for others, age is unspecified) corresponding to the analysis of **Figure 1D,E**.
Data shown as mean ± SEM with data points representing individual animals or persons. Statistics calculated with MWU test (A), ns=nonsignificant.

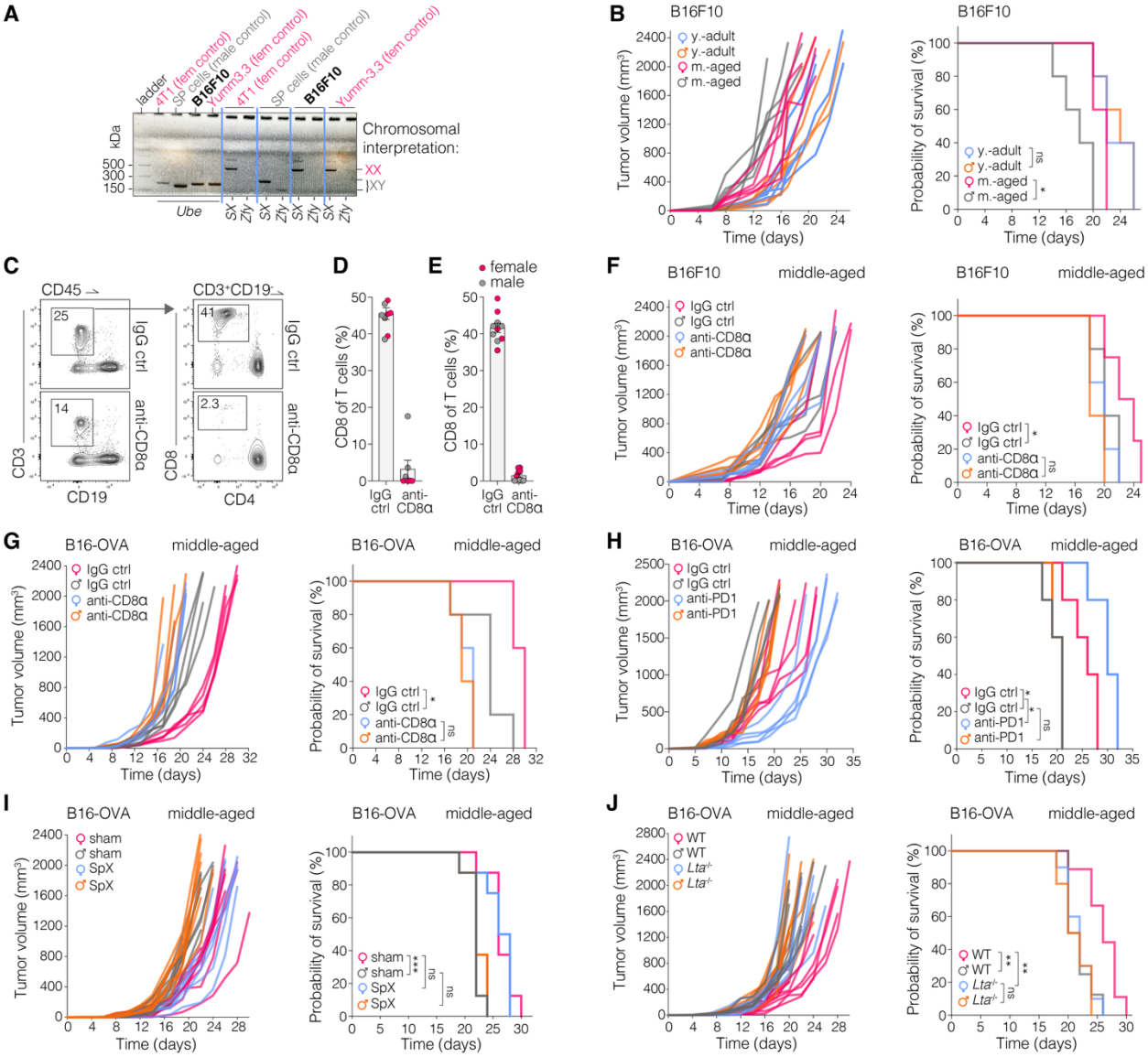

Figure S2. Melanoma tumor model growth analyses.

(A) PCR analysis, *Sly* intron 8 from the Y chromosome and *Xlr* intron 6 from the X chromosome (*SX*, 480/685 bp on XX chromosomes, 280 bp on Y chromosomes). Male control gene *Zfy* and Ubiquitin as general control gene *Uba1/Ube1y1* (Ube, 217 bp). The data show that B16F10 melanoma lack Y chromosome.

(B) B16F10 tumor growth and survival probability in adult and middle-aged mice (n=5-8/group), corresponding to *left* part of **Figure 1F**.

(C) Flow cytometry of PBMCs from mice after treatment with IgG control or anti-CD8 antibody to deplete CD8 T cells.

(D) Quantification of CD8 T depletion, corresponding to **Figure S2F**.

(E) Quantification of CD8 T depletion, corresponding to *middle* part of **Figure 1F** and **Figure S2G**.

(F) B16F10 tumor growth and survival probability in middle-aged mice after CD8 T cell depletion in comparison to controls.

(G) B16-OVA tumor growth and survival probability in adult and middle-aged mice after CD8 T cell depletion, corresponding to *middle* part of **Figure 1F**.

(H) B16-OVA tumor growth and survival probability in middle-aged mice treated with IgG controls or anti-PD1 antibody, corresponding to the *right* part of **Figure 1F**.

(I) B16-OVA tumor growth and survival probability in middle-aged mice after sham surgery or splenectomy (SpX), n=8/group. **(J)** B16-OVA tumor growth in middle-aged wt or *Lta*$^{-/-}$ mice (n=8-10/group).

Data shown as mean ± SEM with data points representing individual animals. Statistics calculated with Log-rank test (B,F,G,H,I,J), ns=nonsignificant, *p<0.05,**p<0.01,***p<0.005**.**

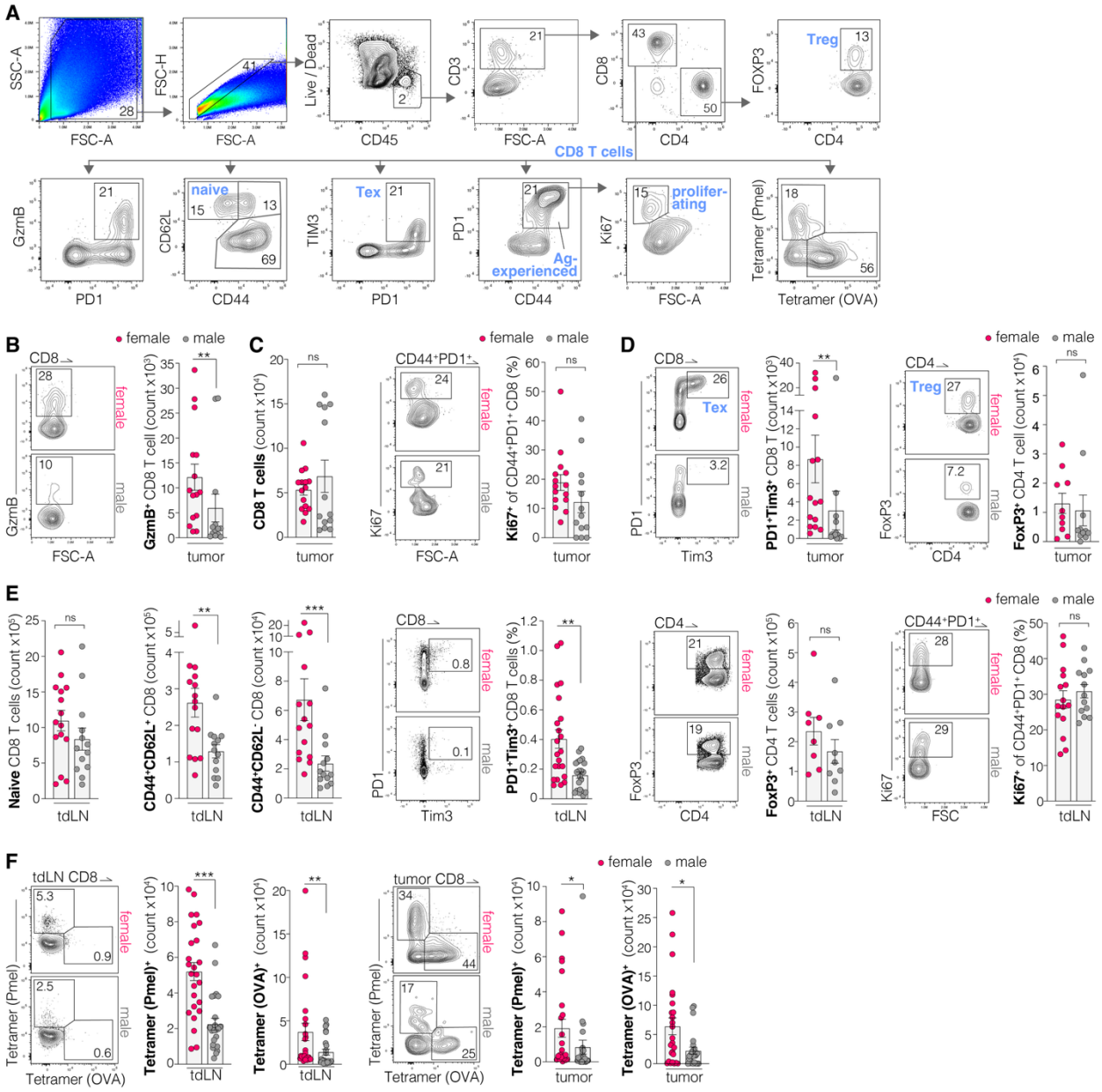

Figure S3. Flow cytometry analysis of the B16 mouse melanoma model.

(A) Flow cytometry gating strategy of lymphocytes in the primary tumor; regulatory T cells (Treg), exhausted T cells (Tex), central memory T cells (Tcm).

(B) Flow cytometry analysis of CD8 T cells from the primary tumor of middle-aged mice implanted with B16-OVA tumors, group matched 13-15 days after implantation (corresponding to **Figure 1E,F,G,H**).

(C) Quantification of CD8 T cell infiltration in the primary tumor and proliferation (Ki67⁺) of antigen-experienced (CD44⁺PD1⁺) CD8 T cells.

(D) Quantification of Tex (Tim3⁺PD1⁺) and Treg (CD4⁺FoxP3⁺) cells in the primary tumor.

(E) Flow cytometry analysis of T cells in the tdLN of middle-aged mice implanted with B16-OVA tumors, group matched 13-15 days after implantation (corresponding to **Figure 1E,F,G,H**).

(F) Flow cytometry analysis of tetramer staining from primary melanomas and their draining LNs. Data points include the control sham/vehicle groups of middle-aged mice from thymectomy, gonadectomy and Degarelix treatment experiments (**Figure S12A, Figure S14C,G**).

Data shown as mean ± SEM with data points representing individual animals. Statistics calculated with MWU test (A,B,C,D,E,F), ns=nonsignificant, **p<0.01, ***p<0.005.

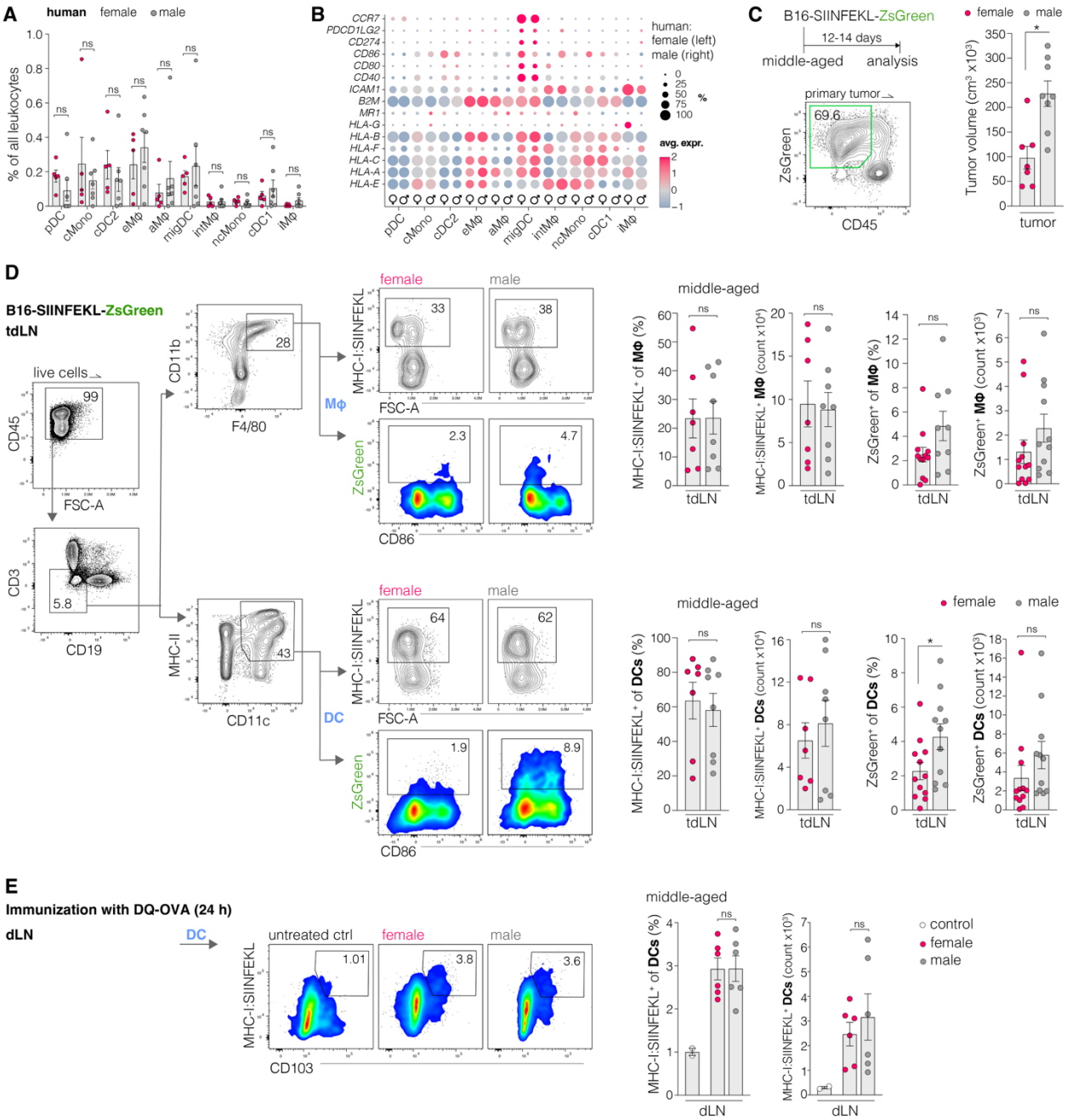

Figure S4. Subset distribution of APCs in human LNs and antigen presentation capacity in murine LNs.
(A) Frequencies of subsets of APC in human LNs (53-73 years of age), scRNA-seq data from Dominguez Conde *et al.*[38] Plasmacytoid dendritic cell (pDC), classical monocytes (cMono), classical DC type 2(cDC2), erythrophagocytic macrophage (eMΦ), alveolar (aMΦ), migratory DC (migDC), intestinal MΦ (intMΦ), non-classical Monocyte (ncMono), classical DC type 1 (cDC1), intermediate MΦ (iMΦ).
(B) Expression levels of functional receptors in APCs of human LNs, females n=5, males n=7.
(C) B16-SIINFEKL-zsGreen tumors implanted in middle-aged mice, volume at day of analysis and representative flow cytometry plot demonstrating presence of zsGreen in tumor cells and in some CD45⁺ leukocytes within the primary tumor. **(D)** Representative plots of the flow cytometry analysis and quantification of DC, MΦ presenting SIINFEKL peptide via MHC-I (MHC-I:SIINFEKL) or carrying tumor antigen (zsGreen) in tdLNs of middle-aged mice with B16-SIINFEKL-zsGreen tumors. **(E)** Representative plots of the flow cytometry analysis and quantification of MHC-I:SIINFEKL⁺ in draining LNs (dLN) of middle-aged mice 25 hours after immunization with DQ-OVA, which identifies antigen processing.
Data shown as mean ± SEM with data points representing individual animals or persons. Statistics calculated with MWU test (A,C,D,E), ns=nonsignificant, *p<0.05.

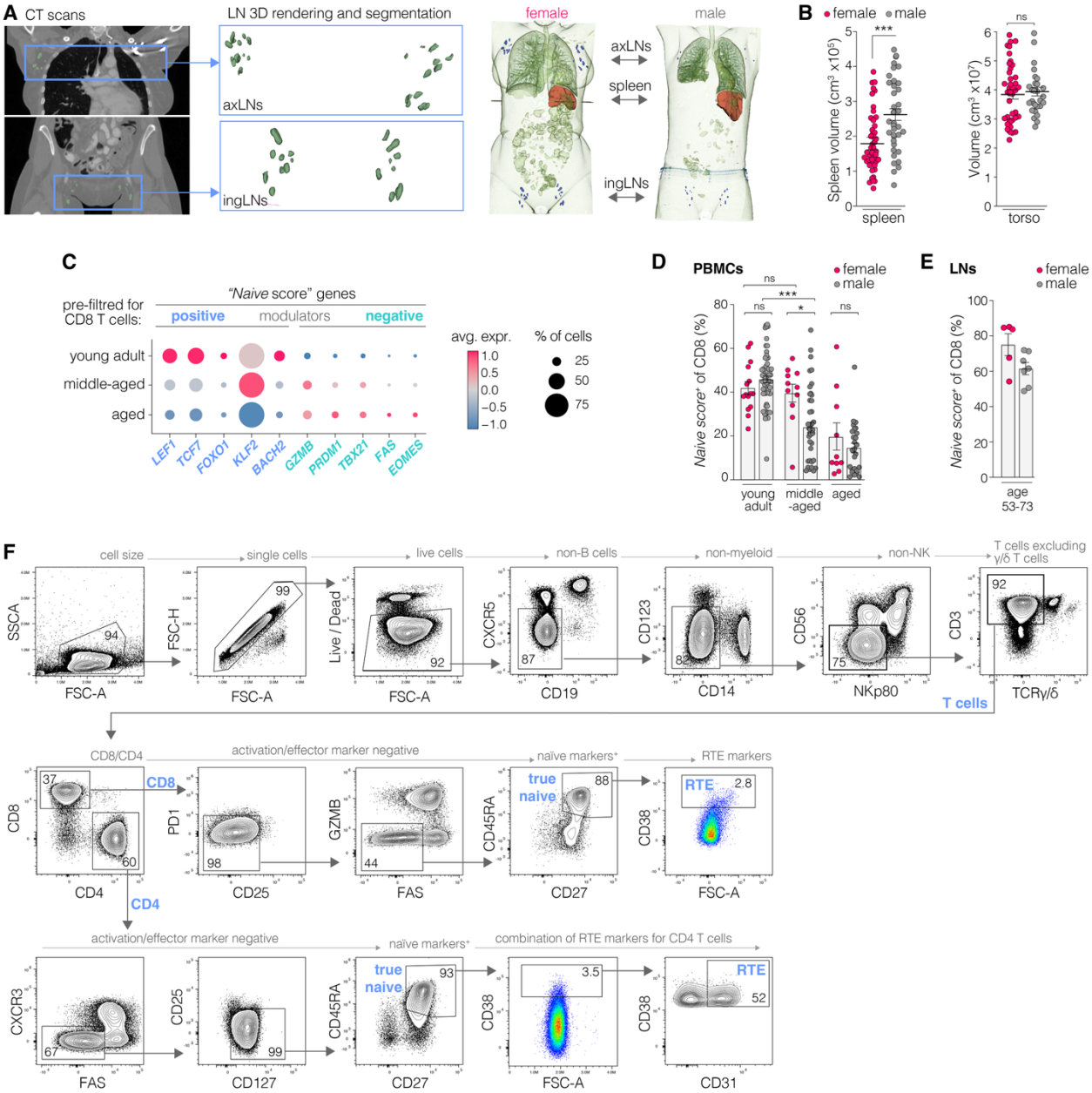

Figure S5. Human LN volumes and naive CD8 T cells.

(A) Schematic representation of LN segmentation, 3D rendering, and quantification of LN volumes based on CT scans from Roth et al. and Rister et al.[81,82].

(B) Data corresponding to **Figure 2A-B**, age of individuals (when available, for others, age is unspecified), the segmented and quantified spleen and torso volumes.

(C) Expression levels of genes included in the "*Naive Score*" with genes that positively or negatively modulate the score.

(D) Quantification of naive CD8 T cells in human peripheral blood mononuclear cells (PBMCs) using the *Naive Score*, based on scRNA-seq data from Terekhova *et al.*[36]

(E) Quantification of naive CD8 T cells in human LNs using the *Naive Score*, based on scRNA-seq data from Dominguez Conde *et al.*[38]

(F) Flow cytometry gating strategy for human PBMCs, including recent thymic emigrants (RTEs), with data derived from Bohacova & Terekhova *et al.*[37]

Data shown as mean ± SEM with data points representing individual animals or human subjects. Statistics calculated with MWU test (B,D), ns=nonsignificant, *p<0.05, ***p<0.005.

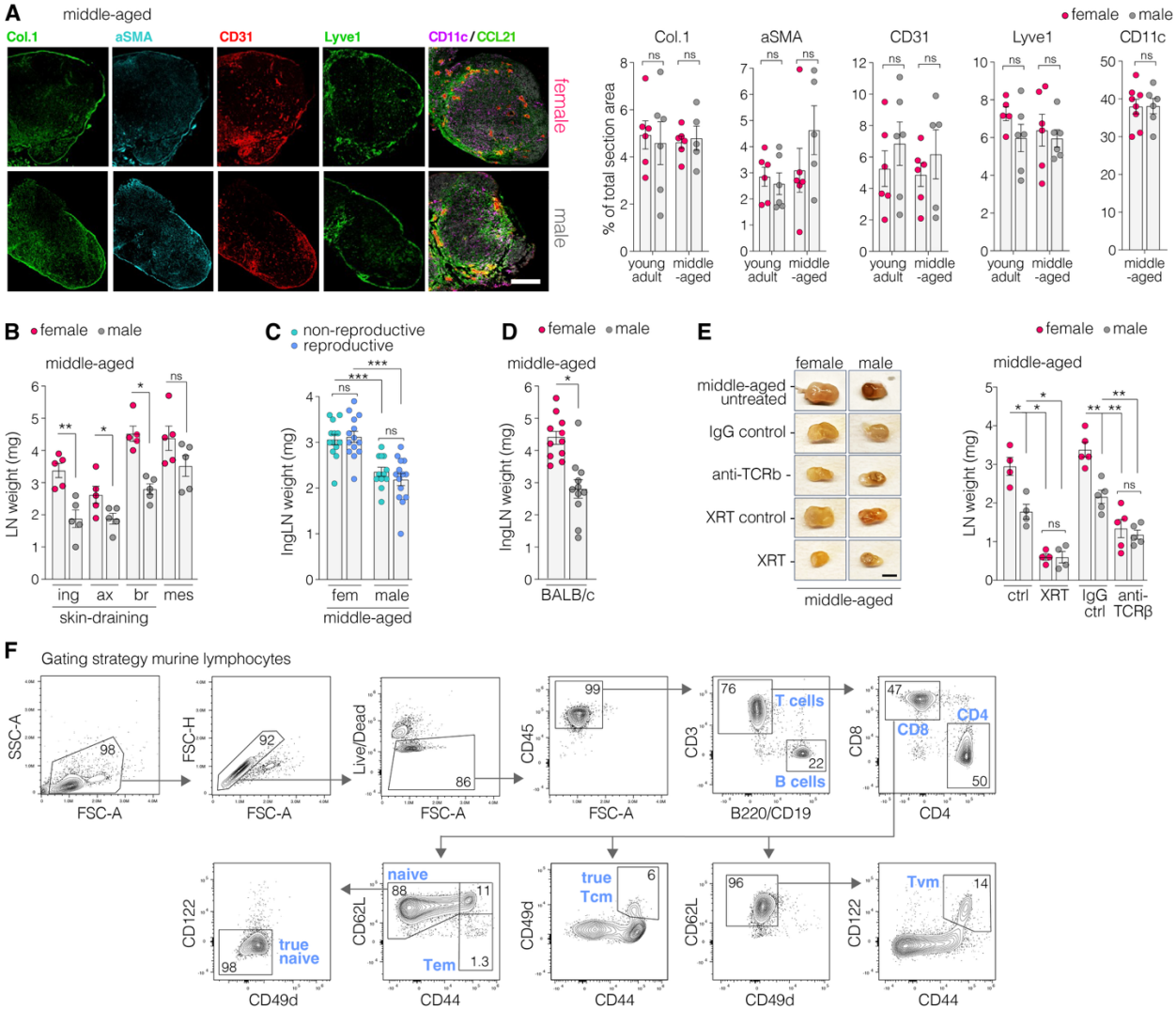

Figure S6. Age-and sex-related contraction of LNs with and without lymphodepletion.
(A) Representative images and quantification of inguinal LN sections from middle-aged mice; Collagen-I (Col.1), alpha smooth muscle actin (αSMA) Scale bar: 200 µm.
(B) Lymph node (LN) weights in different age groups of female and male mice, including inguinal (ing), axillary (ax), brachial (br), and mesenteric (mes) LNs.
(C) Weights of inguinal LNs in non-reproductive and reproductive (retired breeder) female and male mice.
(D) LN weights in middle-aged female and male BALB/c mice.
(E) Representative photographs and weight quantification of inguinal LNs from middle-aged mice treated with irradiation (XRT, sublethal does of 4 Gy) or anti-TCRβ antibody-mediated T cell depletion. Scale bar 500 µm.
(F) Flow cytometry gating strategy for murine lymphocytes, including central memory T cells (Tcm), effector memory T cells (Tem), and virtual memory T cells (Tvm).
Data shown as mean ± SEM with data points representing individual animals or human subjects. Statistics calculated with MWU test (A,B,C,D,E), ns=nonsignificant, *p<0.05, **p<0.01, ***p<0.005.

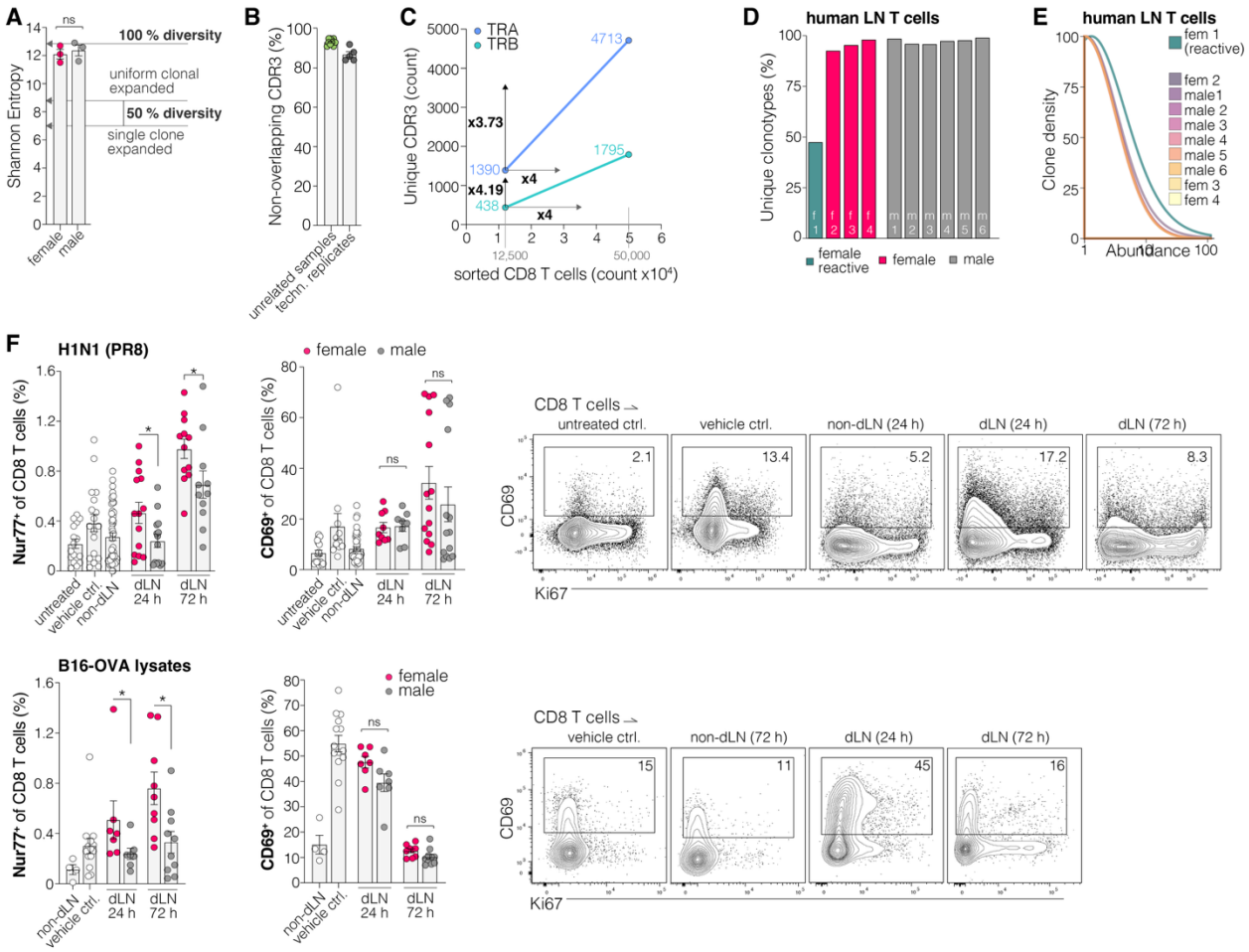

Figure S7. TCR diversity of naive T cells in LNs and T cell activation after immunization in mice.
(A) Shannon Entropy analysis of the TCR repertoire (T cell receptor beta chain, TRB) diversity using bulk TCR sequencing data of CD8 T cells sorted from inguinal LNs of middle-aged mice. Indicated are approximations of theoretical values with 100% diversity and 50 % diversity in reactive LNs with an even clonal expansion or a single expanded clone.
(B) CDR3 (TRB) sequences overlapping with other samples or technical replicates of the same sample.
(C) Bulk TCR sequencing of T cells from the same LN sample (ingLN of middle-aged male) with different CD8 T cell counts (12,500 and 50,000 cells). Indicated are unique CDR3 (TRA, TRB) and the fold change (x...) between samples with different input cell counts. Results show that almost every additional cell in this LN sample equals an additional unique TCR.
(D) scTCR-seq of T cells from human LNs, data set from Dominguez Conde *et al.*[38] Percent of unique clonotypes (including combination of TRA, TRB). One female sample with apparent reactive LN (see **E**).
(E) Clonal density and abundance (arbitrary units) of samples depicted in (**D**).
(F) Flow cytometry analysis of Nur77 and CD69 expression in CD8 T cells 24 or 72 hours after immunization with inactivated H1N1 (PR8) virus particles or B16-OVA tumor cell lysates.
Data shown as mean ± SEM with data points representing individual animals or persons. Statistics calculated with t test (A), MWU test (F), ns=nonsignificant,*p<0.05,***p<0.005.

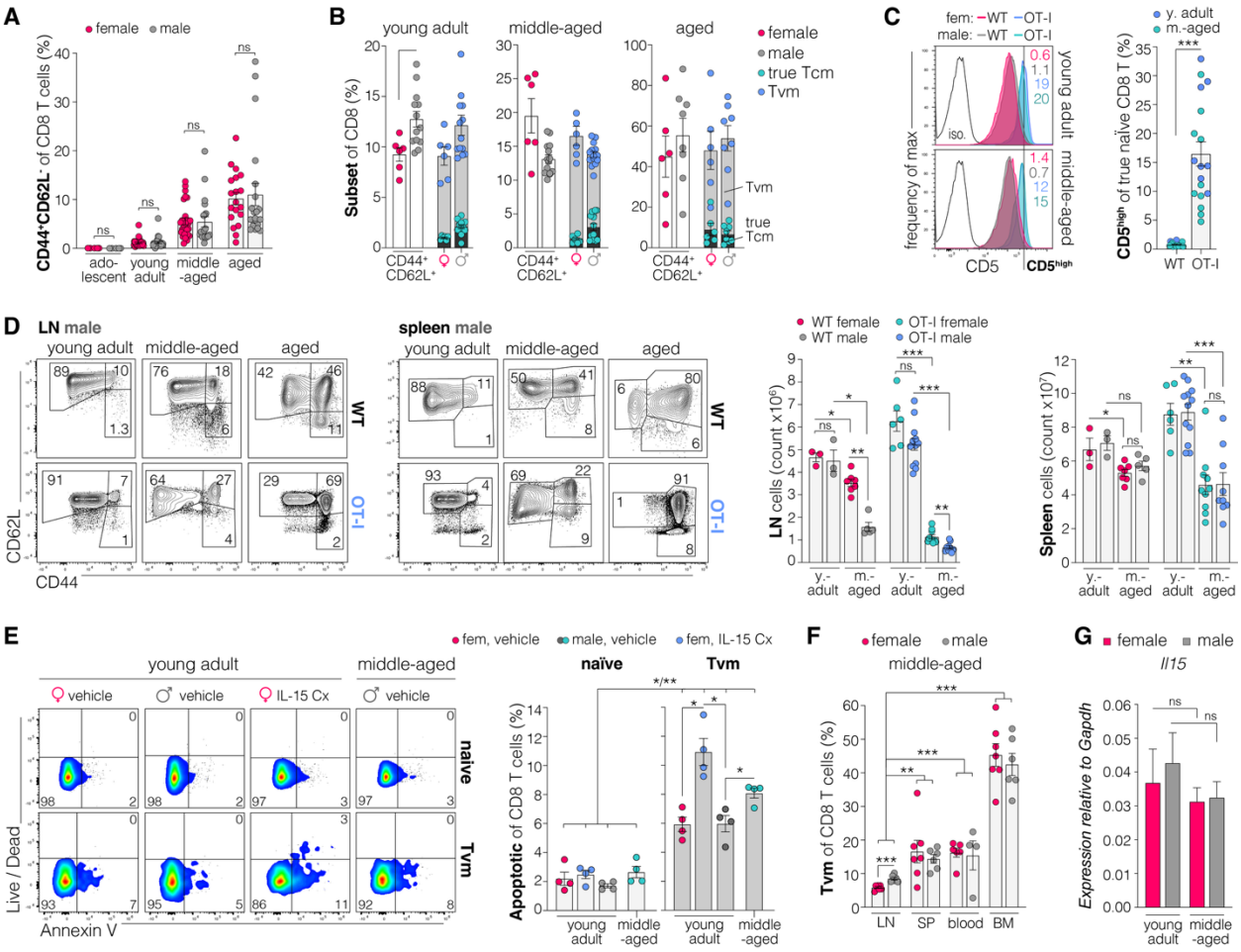

Figure S8. Age group related analysis of naive and memory CD8 T cells in wilt type and OT-1 mice.
(A) Flow cytometry analysis of effector-like (CD44⁺CD62L⁻) CD8 T cells in LNs of wild-type (WT) mice.
(B) Quantification of flow cytometry analysis of CD8 T cells from the ingLN of adult, middle-aged and aged mice from **Figure 3C,D** show that CD44⁺CD62L⁺ contain both true Tcm and virtual memory (Tvm) cells, with a majority being Tvm.
(C) Histograms of CD5 expression in true naive CD8 T cells and quantification of CD5^{high} cells from ingLNs of WT or OT-I mice, young adults (y. adult) and middle-aged (m.-aged).
(D) Representative flow cytometry plots CD8 T cells and quantification of total cell count of ingLNs and spleen of WT and OT-I mice.
(E) Flow cytometry analysis of Live/Dead (Zombie UV) a Annexin-V staining in true naive or Tvm cells of adult mice after treatment with vehicle solution or IL-15 Cx or middle-aged males. Analysis 4 weeks after end of treatment.
(F) Flow cytometry analysis of Tvm CD8 T cells in LNs, spleen (SP), blood and bone marrow (BM).
(G) qPCR gene expression analysis of *Il15* relative to *Gapdh* in murine ingLN, n=10-15/group.
Data shown as mean ± SEM with data points representing individual animals. Statistics calculated with MWU test (A,C,D, E,F,G), ns=nonsignificant, *p<0.05, **p<0.01, ***p<0.005.

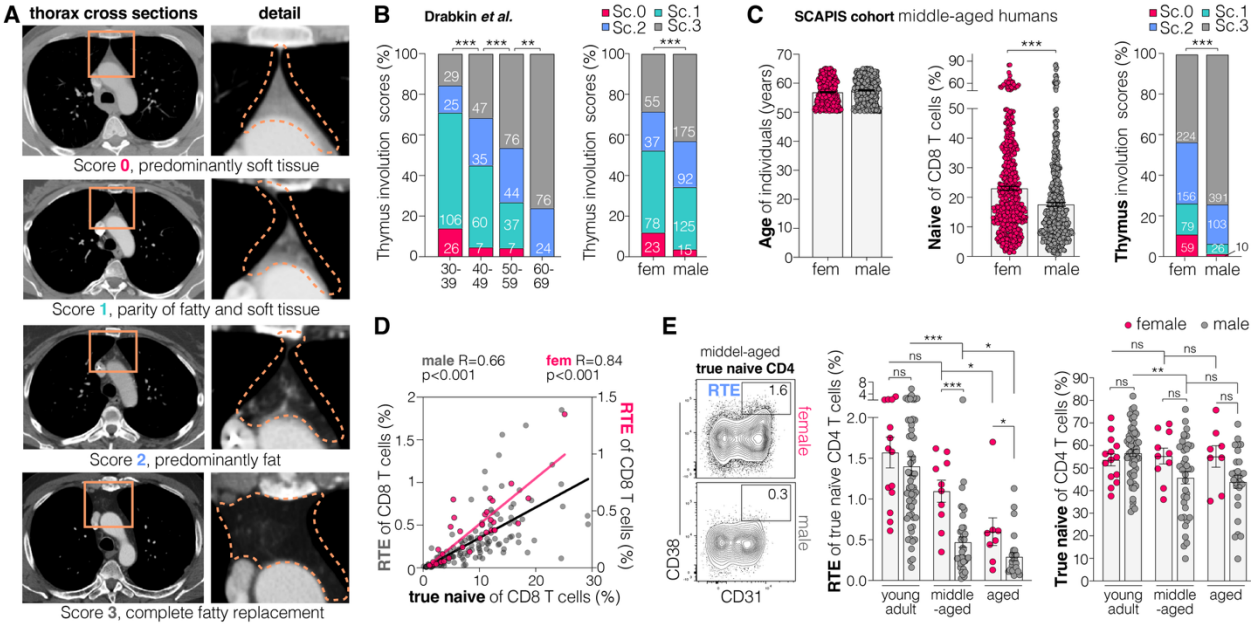

Figure S9. Human thymus and circulating recent thymic emigrants.

(A) Representative images of CT scans and scores to evaluate the involution of human thymuses, score 0: predominantly soft tissue; score 1: parity of fatty and soft tissue; score 2: predominantly fat; score 3: complete fatty replacement.

(B) Data published by Drabkin *et al.*[56] confirming age-related thymus involution using the scoring system as described in (a). Numbers in columns indicate number of individuals per group.

(C) Age in years (all middle-aged, 50-65 years old), proportion of naive CD8 T cells within the CD8 T cell compartment in blood samples and thymus involution scores of the SCAPIS cohort of middle-aged individuals, n=530 females and 518 males.

(D) Correlation of the frequency of the true naive subset and of RTE relative to CD8 T cells, public data set[37].

(E) Representative flow cytometry plot and quantification of CD4 RTE and true naive CD4 T cells in human blood, public data set[37]. Gating strategy in **Figure S5F**.

Data shown as mean ± SEM with data points representing individual animals. Statistics calculated with Fisher's exact test (B, C), Pearson correlation (D), MWU test (C,E), ns=nonsignificant, *p<0.05, **p<0.01, ***p<0.005.

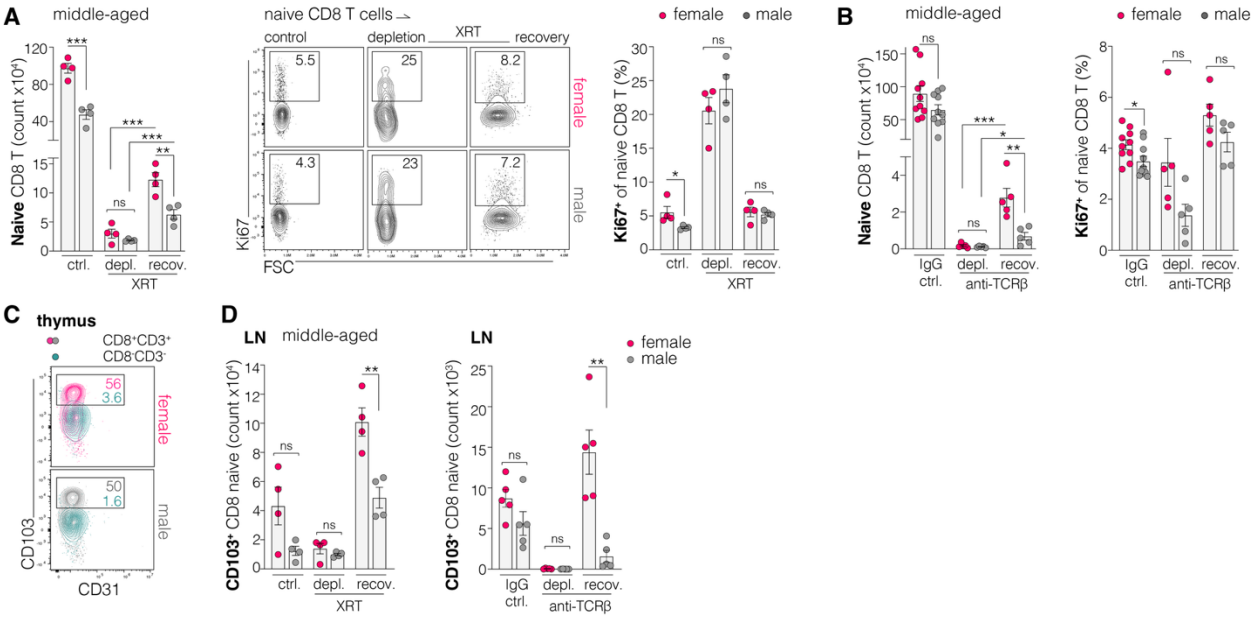

Figure S10. T cell recovery after experimental lymphodepletion and thymocyte alterations during aging.
(A) Flow cytometry analysis of naive CD8 T cells and proliferation of naive T cells (Ki67⁺) in middle-aged untreated control mice or after irradiation (XRT, sublethal dose with 4 Gy) induced lympho-depletion (depl., day 7) and after a period of recovery (recov., day 28).
(B) Flow cytometry analysis of naive CD8 T cells and proliferation of naive T cells (Ki67⁺) in middle-aged mice in IgG control treatment or after anti-TCRß (T cell receptor beta chain) antibody mediated T cell depletion (depl., day 7) and after a period of recovery (recov., day 19).
(C) Representative flow cytometry plots of CD103 expression (as indicator of RTEs) in single positive (SP) $CD8^+CD3^+$ thymocytes right before egress to periphery and $CD8^-CD3^-$ as gating controls.
(D) $CD103^+$ RTEs in the periphery analyzed by flow cytometry of ingLNs from middle-aged mice after XRT or anti-TCRß antibody mediated T cell depletion (day 7) and after a period of recovery (day 28).
Data shown as mean ± SEM with data points representing individual animals. Statistics calculated with MWU test (A,B,D), ns=nonsignificant, *p<0.05, **p<0.01, ***p<0.005.

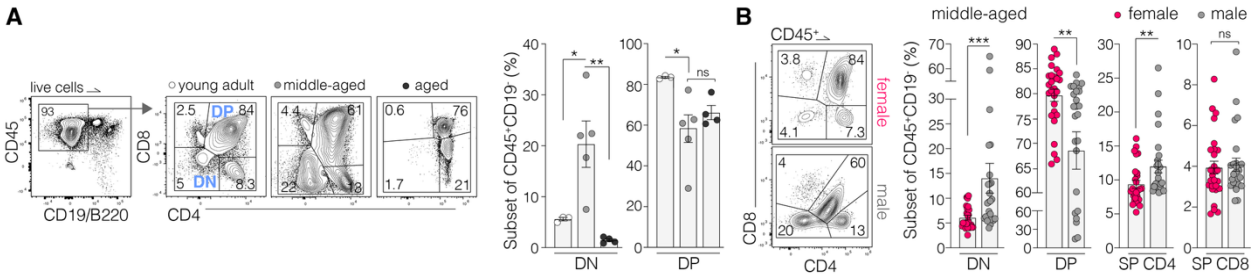

Figure S11. Age-related thymus atrophy is characterized by higher proportions of double negative thymocytes in middle-aged mice.

(A) Flow cytometry analysis of thymocytes ($CD45^{+}CD19^{-}$) in males of different age groups; including double negative (DN) and double positive (DP) cells.

(B) Flow cytometry analysis of thymocytes ($CD45^{+}CD19^{-}$) in middle-aged female and male mice; including DN and DP cells and single positive (SP) cells.

Data shown as mean ± SEM with data points representing individual mice. Statistics calculated with MWU test (A,B), ns=nonsignificant, *p<0.05, **p<0.01, ***p<0.005.

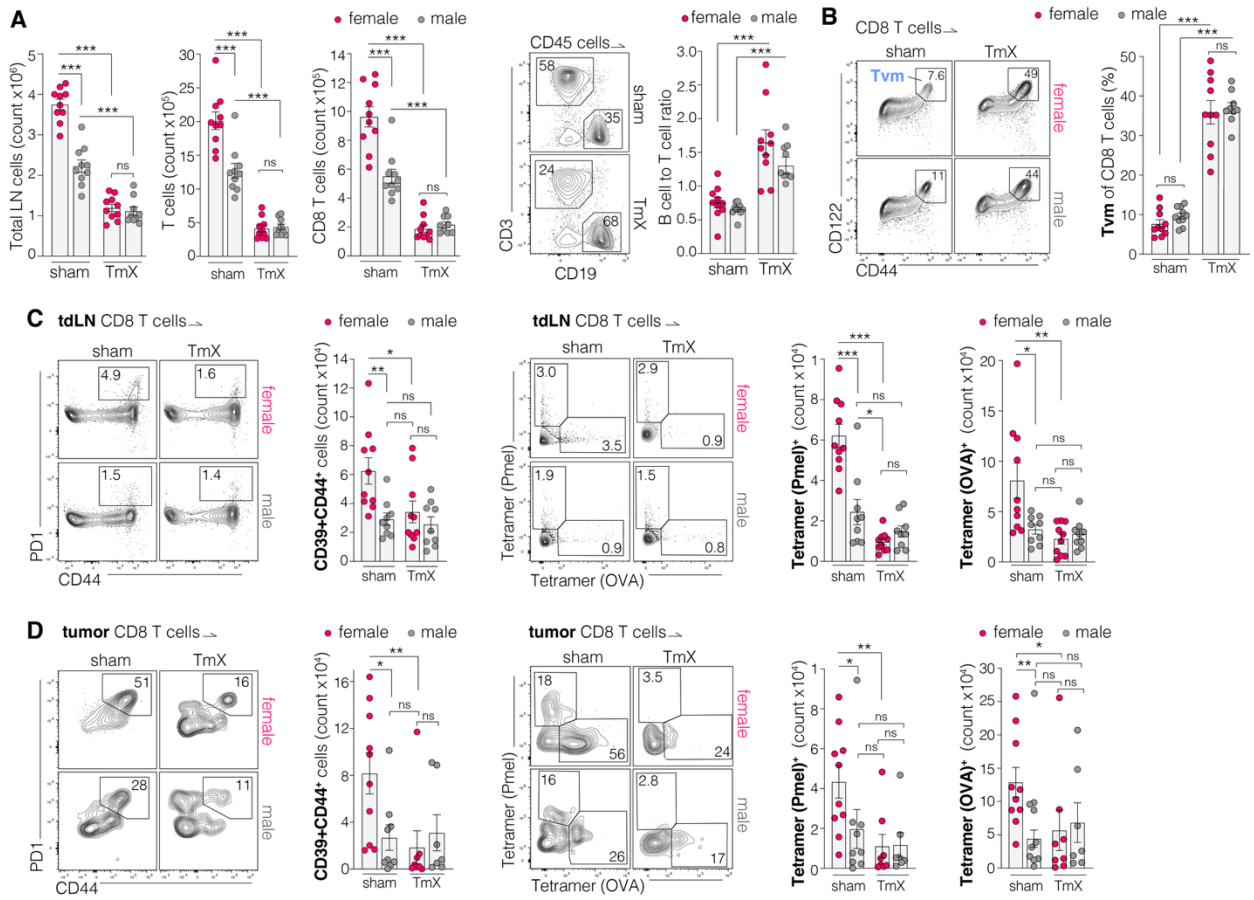

Figure S12. Consequences of thymectomy for LNs and tumor recognition in tdLN and within the primary tumor.
(A) Quantification of total LN cells, T cells, CD8 T cells and the T cell to B cell ratio in ingLNs of middle-aged sham and TmX treated mice.
(B) Flow cytometry analysis of virtual memory CD8 T cells from ingLNs of middle-aged sham and TmX mice.
(C) Flow cytometry analysis of CD8 T cells in tdLNs of sham and TmX mice with B16-OVA tumors. Corresponding to Figure 5K,L,M.
(D) Flow cytometry analysis of CD8 T cells from the primary B16-OVA tumor of sham and TmX mice. Corresponding to Figure 5K,L,M.
Data shown as mean ± SEM with data points representing individual animals. Statistics calculated with MWU test (A,B,C,D), ns=nonsignificant, *p<0.05, **p<0.01, ***p<0.005.

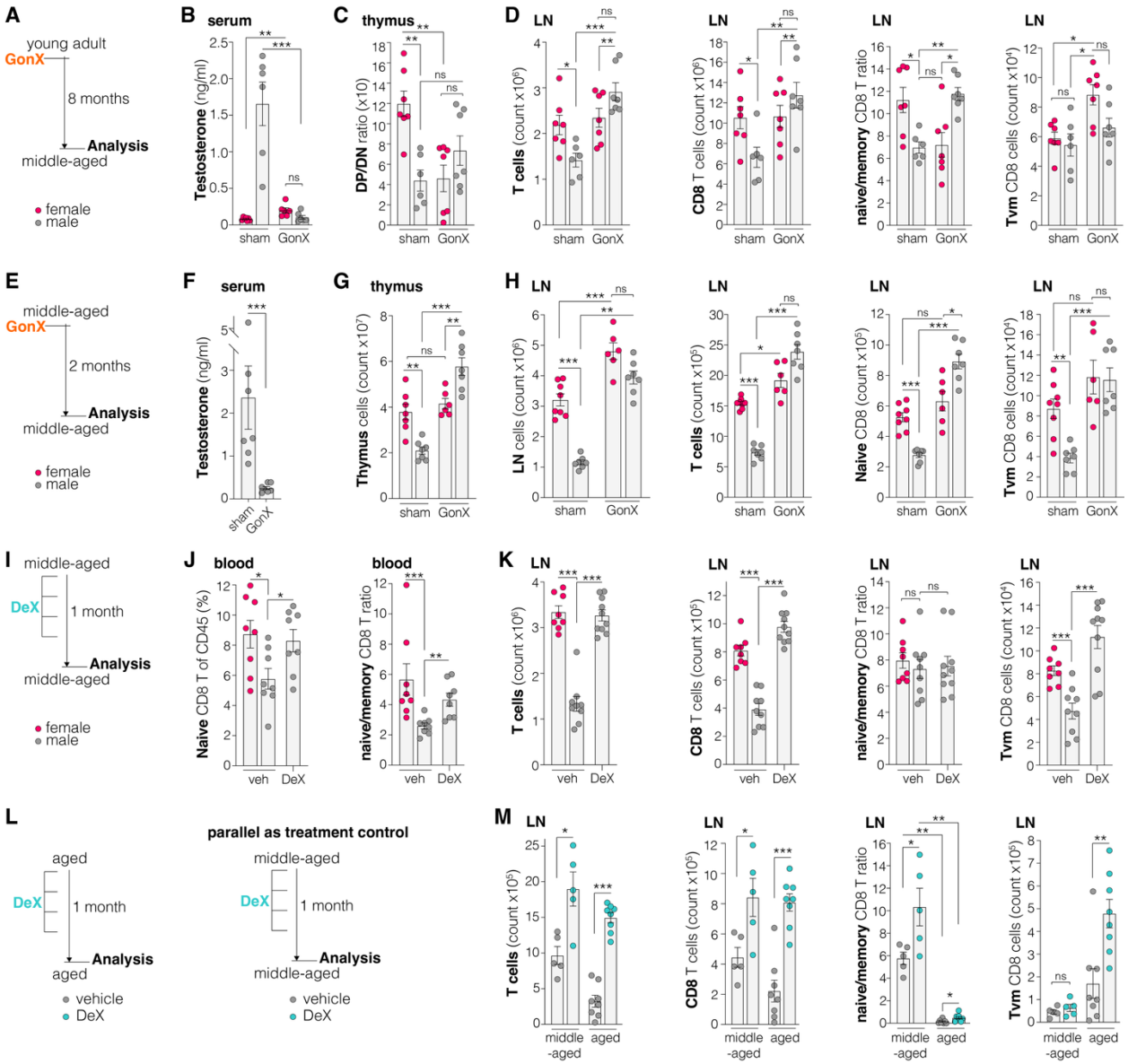

Figure S13. Consequences of sex steroid ablation for the thymus and lymph nodes.
(A) Experimental set up, Gonadectomy (GonX) in adult mice and analysis middle-aged.
(B) Analysis of serum Testosterone levels.
(C) Flow cytometry analysis of thymocytes ($CD45^{+}CD19^{-}$); ratio of double positive (DP) and double negative (DN) cells.
(D) Flow cytometry analysis and quantification of T cells from tumor-naive LNs.
(E) Experimental set up, GonX in middle-aged mice and analysis two month after surgery.
(F) Analysis of serum Testosterone levels.
(G) Number of total thymocytes.
(H) LN cellularity and flow cytometry analysis of T cells from tumor-naive LNs.
(I) Experimental set up, Degarelix (DeX) in middle-aged mice and analysis one month after beginning of treatment.
(J) Flow cytometry analysis of naive and memory CD8 T cells in blood samples.
(K) Flow cytometry analysis of T cells from tumor-naive LNs.
(L) Experimental set up, DeX in aged male mice and analysis one month after beginning of treatment, in parallel DeX treatment of middle-aged males as treatment controls.
(M) Flow cytometry analysis of T cells from tumor-naive LNs.
Data shown as mean ± SEM with data points representing individual animals. Statistics calculated with MWU test (B,C,D,F,G,H,J,K,M), ns=nonsignificant, *p<0.05, **p< 0.01, ***p<0.005.

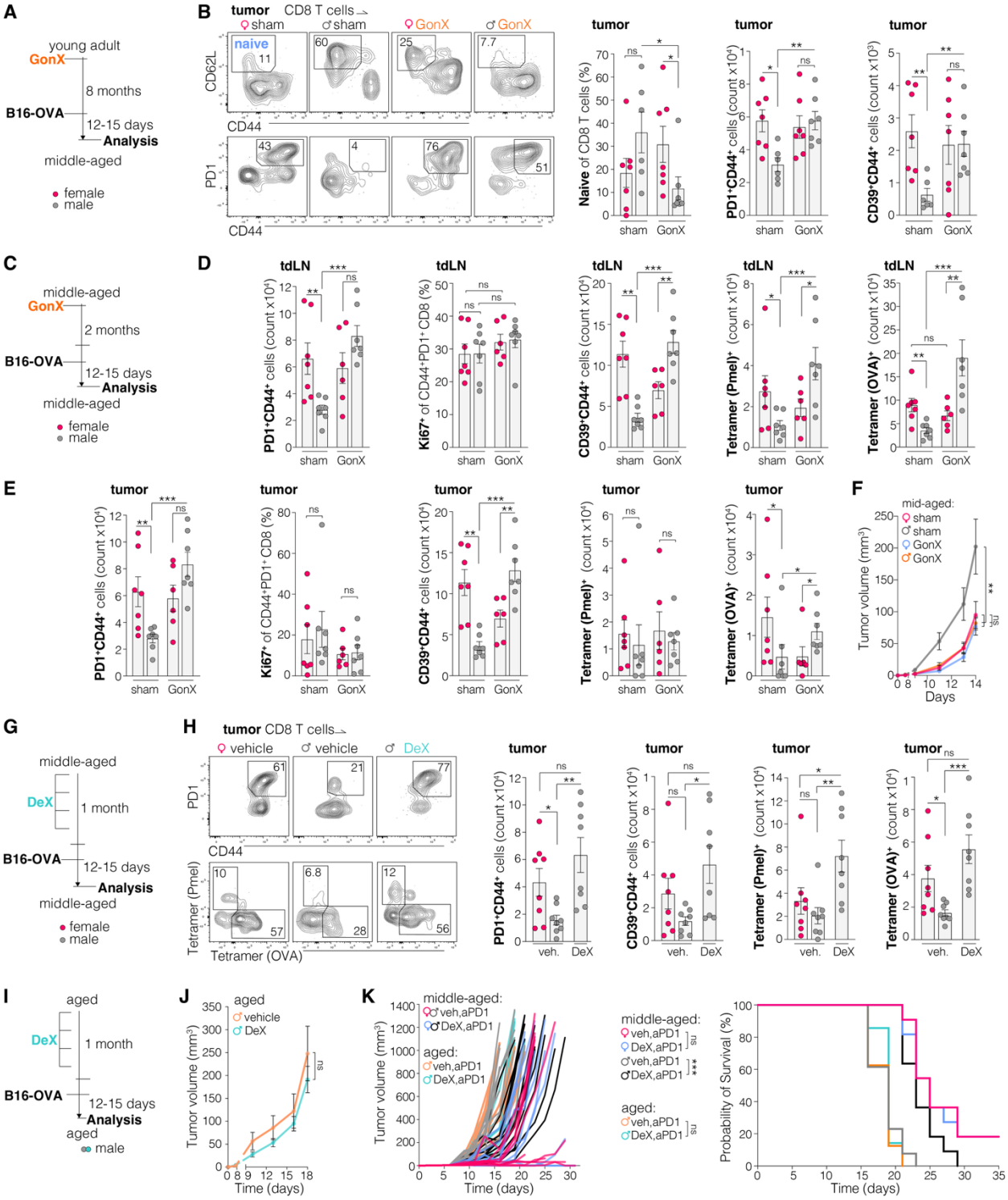

Figure S14. Consequences of sex steroid ablation tumor recognition in tdLNs and the primary tumor.
(A) Experimental set up, gonadectomy (GonX) in adults, B16-OVA tumor implantation and analysis in middle-aged mice.
(B) Flow cytometry analysis of T cells in tumors.
(C) Experimental set up, GonX in middle-aged mice and analysis two month after surgery.
(D) Flow cytometry analysis of tdLNs and
(E) TILs.
(F) B16-OVA tumor growth in mice after sham or GonX surgery, n=7/group.

(G) Experimental set up, degarelix (DeX) treatment in middle-aged mice, B16-OVA tumor implantation and analysis.
(H) Flow cytometry analysis of TILs.
(I) Experimental set up, DeX treatment in aged mice.
(J) B16-OVA tumor growth in vehicle or DeX treated aged mice (n=4-5/group).
(K) B16-OVA tumor growth and survival probability in middle-aged and aged mice after treatment with DeX and anti-PD1 (n=7-13/group).
Data shown as mean ± SEM with data points representing individual animals. Statistics calculated with MWU test (B,D,E,H), 2-way ANOVA (F,J) or Log-rank test (K) ns=nonsignificant, *p<0.05, **p<0.01, ***p<0.005).

Table S1. Antibodies, tetramers, dyes

Epitope	Fluorophore	Reactivity	Manufacturer	Clone	Cat. #	RRID
Annexin-V	PE		BioLegend		640907	
B220	AF647	mouse	BioLegend	RA3-6B2	103229	AB_389330
B220	APC/Cy7	mouse	BioLegend	RA3-6B2	103223	AB_313006
B220	PE	mouse	BioLegend	RA3-6B2	103207	AB_312992
CD11b	AF 700	mouse	BioLegend	M1/70	101222	AB_493705
CD11c	APC	mouse	BioLegend	N418	117309	AB_313778
CD122	PE	mouse	BioLegend	TM-β1	123209	AB_940617
CD122	PE/Cy5	mouse	BioLegend	TM-β1	123219	AB_2715961
CD127	PE/Cy5	mouse	BioLegend	A7R34	135015	AB_1937261
CD127	FITC	mouse	BioLegend	A7R34	135007	AB_1937231
CD16/CD32	purified	mouse	BioLegend	93	101301	AB_312800
CD19	FITC	mouse	BioLegend	6D5	115505	AB_313640
CD19	AF700	mouse	BioLegend	1D3/CD19	152414	AB_2922474
CD25	PE	mouse	BioLegend	PC61	102007	AB_312856
CD3	FITC	mouse	BioLegend	17A2	100203	AB_312661
CD3	PE/Dazzl493	mouse	BioLegend	17A2	100246	AB_2565882
CD3	PerCP	mouse	BioLegend	17A2	100217	AB_1595492
CD39	PE/Cy7	mouse	BioLegend	Duha59	143805	AB_2563393
CD4	APC/Cy7	mouse	BD Bioscience	GK1.5	561830	AB_10897172
CD4	BV605	mouse	BioLegend	RM4-5	100547	AB_11125962
CD4	BV650	mouse	BioLegend	RM4-5	100551	AB_2563053
CD4	APC	mouse	BioLegend	RM4-5	100515	AB_312718
CD44	APC	mouse	BioLegend	IM7	103011	AB_312962
CD44	BV750	mouse	BioLegend	IM7	103037	AB_10900641
CD44	PE	mouse	BioLegend	IM7	103023	AB_312958
CD45	BV510	mouse	BioLegend	30-F11	103137	AB_2561392

CD45	PE/Dazzl493	mouse	BioLegend	30-F11	103145	AB_2564002
CD45	AF700	mouse	BioLegend	30-F11	103127	AB_493714
CD45	PE	mouse	BioLegend	30-F11	103105	AB_312970
CD45	PerCP	mouse	BioLegend	30-F11	103129	AB_893343
CD49d	FITC	mouse	BioLegend	R1-2	103605	AB_313036
CD49d	PE	mouse	BioLegend	R1-2	103607	AB_313039
CD5	AF700	mouse	BioLegend	53-7.3	100635	AB_2687001
CD62L	PE	mouse	BioLegend	MEL-14	104407	AB_313094
CD62L	BV421	mouse	BioLegend	MEL-14	104435	AB_10900082
CD62L	AF700	mouse	BioLegend	MEL-14	104426	AB_493719
CD69	FITC	mouse	BioLegend	H1.2F3	104505	AB_313108
CD69	AF700	mouse	BioLegend	H1.2F3	104539	AB_2566304
CD8a	Spark-UV387	mouse	BioLegend	53-6.7	100797	AB_2922451
CD8a	PE/Cy7	mouse	BioLegend	53-6.7	100721	AB_312760
CD8a	Spark-YG593	mouse	BioLegend	QA17A07	155023	AB_2892316
CD8a	FITC	mouse	BioLegend	53-6.7	100705	AB_312744
CD8a	PE	mouse	BioLegend	53-6.7	100707	AB_312747
F4/80	PerCP/Cy5.5	mouse	BioLegend	BM8	123127	AB_893484
FoxP3	PerCP/Cy5.5	mouse	eBioscience	FJK-16s	45577382	AB_914351
Gp100 (Pmel)	PE	mouse	abcam	EP4863(2)	ab246731	AB_2732921
Ki67	BV650	mouse	BioLegend	11F6	151215	AB_2876504
Ki67	PE/Cy7	mouse	BD Bioscience	B56	561283	AB_10716060
Ki67	BV510	mouse	BioLegend	B56	563462	AB_2738221
MHC-I:SIINFEKL	PE	mouse	BioLegend	25-D1.16	141603	AB_10895905
MHC-I:SIINFEKL	APC	mouse	BioLegend	25-D1.16	141605	AB_11219402
MHC-II	AF647	mouse	BioLegend	M5/114.15.2	107617	AB_493525
Nur77	AF594	mouse	BioLegend	1E10A15	653504	AB_2563321
Nur77	PE	mouse	Miltenyi	REA704	130111417	AB_2653071
PD1	BV785	mouse	BioLegend	29F.1A12	135225	AB_2563680
PD1	PE	mouse	BioLegend	29F.1A12	135205	AB_1877231
PD1	APC	mouse	BioLegend	29F.1A12	135209	AB_2159183
TCRb	BV711	mouse	BioLegend	H57-597	109243	AB_2629564
TCRb (InVivoMAb)	purified	mouse	BioXcell	H57-597	#BE0102	AB_10950158
Tetramer gp100 (25-33)	AF647	mouse	NTCF (NIH)	EGSRNQDWL	#71998	
Tetramer OVA (257-264)	BV421	mouse	NTCF (NIH)	SIINFEKL	#73246	

Tim-3	BV711	mouse	BioLegend	RMT3-23	119727	AB_2716208
Tim-3	APC/Fire750	mouse	BioLegend	RMT3-23	119737	AB_2810367
Zombie-Red Live Dead			BioLegend		423109	
Zombie-UV Live Dead			BioLegend		423108	
Gzmb	APC	mouse	BioLegend	QA16A02	372203	AB_2687027
Gzmb	FITC	mouse	BioLegend	QA16A02	372205	AB_2687029
B220	BV711	mouse	BioLegend	RA3-6B2	103255	AB_2563491

Table S2. Primers and probes. Abbreviations: sjTREC (signal joint T cell receptor excision circle), Fw. (forward), rev. (revers).

Gene	**5'-...-3'**	**Sequence**
sjTREC (mouse)	primer fw.:	CCAAGCTGACGGCAGGTTT
	primer rev.:	AGCATGGCAAGCAGCACC
	probe:	FAM/TGCTGTGTG/ZEN/CCCTGCCCTGCC/3IABkFQ/
SX (mouse)	primer fw.:	GATGATTTGAGTGGAAATGTGAGGTA
	primer rev.:	CTTATGTTTATAGGCATGCACCATGTA
Zfy (mouse)	primer fw.:	GACTAGACATGTCTTAACATCTGTCC
	primer rev.:	CCTATTGCATGGACTGCAGCTTATG
Ube (mouse)	Primer Fw.:	TGGTCTGGACCCAAACGCTGTCCACA
	Primer Rev.:	GGCAGCAGCCATCACATAATCCAGATG
TREC (human)	Primer Fw.:	CACATCCCT TTCAACCATGCT
	Primer Rev.:	GCCAGCTGCAGGGTTTAG G
	Probe:	ACACCTCTGTTTTTGTAAAGGTGC CCACT